Raichu-RhoA, which comprises N-terminal yellow fluorescent protein (YFP), the Rho-binding domain of protein kinase N, RhoA and C-terminal cyan fluorescent protein (CFP). GTP loading into the RhoA domain of Raichu-RhoA protein results in an intramolecular conformational change of Raichu-RhoA, which increases FRET efficiency. By fluorescent microscopic observation, we could localize RhoA activation sites within cells. In HUVEC, RhoA was activated in both the intracellular vesicular compartment and the plasma membrane, with intense signals at cell-cell contacts (**Fig. 4d** and **Supplementary Video 7**). A substantial portion of the intracellular FRET signal coincided with mRFP-2 × FYVE signals (**Fig. 4e**). C2α knockdown reduced the RhoA FRET signal in both the endosomes and the plasma membrane (**Fig. 4d–g** and **Supplementary Video 8**), indicating that C2α is necessary for RhoA activation in PtdIns(3)P-enriched endosomes and in the plasma membrane. We further studied the role of C2α in VEGF receptor internalization, which might occur upstream of RhoA activation[33]. VEGF-A stimulated the internalization of VEGFR2 into the 2 × FYVE$^+$ vesicular compartment, which was dampened by C2α depletion (**Fig. 4h**). VEGF-A induced phosphorylation of VEGFR2 at the plasma membrane 2 min after stimulation; at 30 min after stimulation, most phosphorylated VEGFR2 was redistributed in the intracellular compartment, primarily in early endosome antigen 1 (EEA1)$^+$ endosomes (**Supplementary Fig. 17**). C2α depletion did not inhibit the initial VEGFR2 phosphorylation in the plasma membrane but did inhibit the internalization of phosphorylated VEGFR2 (**Supplementary Fig. 17**). Furthermore, treatment with dynasore, an inhibitor of dynamin-dependent endocytosis[34], inhibited growth-factor–induced RhoA activation, VE-cadherin assembly at cell junctions and tube formation (**Supplementary Fig. 18a–d**). Thus, C2α is essential for the internalization of activated VEGF receptors, activation of RhoA and other signaling molecules on endosomes, RhoA-dependent trafficking and assembly of VE-cadherin at cell junctions.

Endothelial C2α is essential for pathological angiogenesis

We next studied the role of endothelial C2α in pathological angiogenesis using postischemic and tumor angiogenesis models. In *Pik3c2a*$^{i\Delta EC}$ mice, the recovery of blood flow in the ischemic hindlimb after surgical femoral arteriectomy was suppressed during postoperative days 14–28 compared to the recovery in control *Pik3c2a*$^{flox/flox}$ mice ($P < 0.0001$ on day 28; **Fig. 5a**). Immunofluorescence staining using a CD31-specific antibody showed an approximately 50% decrease in microvessel density in the ischemic muscle of *Pik3c2a*$^{i\Delta EC}$ mice compared to control mice on postoperative day 28 ($P < 0.0001$; **Fig. 5b**).

After implantation of Lewis lung carcinoma (LLC) or B16-BL6 melanoma tumors, *Pik3c2a*$^{i\Delta EC}$ mice had diminished tumor volumes and weights compared with those of control *Pik3c2a*$^{flox/flox}$ mice ($P < 0.05$; **Fig. 5c**). The microvessel density in LLC tumors was reduced in *Pik3c2a*$^{i\Delta EC}$ mice compared to that in control mice ($P < 0.05$; **Fig. 5d**). Moreover, double immunostaining with CD31- and NG2-specific antibodies revealed that tumor microvessels in *Pik3c2a*$^{i\Delta EC}$ mice had poor coverage with NG2$^+$ pericytes, which were frequently rounded or detached from the microvessels (**Fig. 5e**).

C2α is required for vascular barrier function and integrity

The permeability of a monolayer of C2α-depleted HUVEC was increased under both resting and VEGF-A–stimulated conditions compared with that of control cells under the same conditions ($P < 0.05$; **Fig. 6a**). After VEGF-A injection, the increase in the leakage of intravenously administered Evans blue dye into the skin was greater in *Pik3c2a*$^{+/-}$ mice than in wild-type mice ($P < 0.05$; **Fig. 6b**). We next studied vascular responses to other hyperpermeability- and inflammation-eliciting insults in global *Pik3c2a*$^{+/-}$ and wild-type mice. Intravenous (i.v.) injection of a low dose of platelet-activating factor (PAF), a mediator of anaphylactic shock[35], did not affect survival in wild-type mice, whereas it induced death in all *Pik3c2a*$^{+/-}$ littermates within 40 min, with accompanying increases in hematocrit levels and Evans blue leakage in the lung (**Fig. 6c,d**). A higher dose of PAF, which induced death in a portion (about 30%) of wild-type mice, caused more rapid death of all *Pik3c2a*$^{+/-}$ mice (**Fig. 6c**). PAF-induced increases in plasma histamine and interleukin-4 (IL-4) concentrations, both of which are anaphylactic mediators, were similar in wild-type and *Pik3c2a*$^{+/-}$ mice (**Supplementary Fig. 19**), suggesting that C2α deficiency impairs endothelial function, resulting in vascular barrier disruption.

Chronic Ang II infusion induced more robust hyperpermeability in the aorta and coronary vessels in *Pik3c2a*$^{+/-}$ mice than in wild-type littermates (**Fig. 6e**). En face immunostaining of the aorta using a VE-cadherin–specific antibody showed disorganization of adherens junctions in AngII-treated *Pik3c2a*$^{+/-}$ mice (**Fig. 6f**). Concomitantly, we found a higher incidence of aortic aneurysms with dissection, resultant rupture and death in *Pik3c2a*$^{+/-}$ mice compared with wild-type littermates (aneurysm occurred in 23/48 *Pik3c2a*$^{+/-}$ mice and 5/44 wild-type mice) ($P < 0.01$; **Fig. 6g,h**). Conditional endothelial-cell–specific deletion of C2α also resulted in a higher occurrence of dissecting aneurysms compared to control mice (aneurysm occurred in 5/20 *Pik3c2a*$^{i\Delta EC}$ mice and 1/13 control mice) ($P < 0.01$; **Fig. 6g**). There was no difference in blood pressure between AngII-treated *Pik3c2a*-deleted and control mice (data not shown). Thus, the aortic walls of C2α-deficient mice seem to be fragile compared with those of wild-type mice. Ang II infusion stimulated matrix metalloproteinase 2 (MMP-2) and MMP-9 activities, which have been implicated in the formation of aneurysms in aortic tissue[6,7,36,37]; these increases were greater in *Pik3c2a*$^{+/-}$ mice than in wild-type mice ($P < 0.05$; **Fig. 6i**). Immunostaining using an antibody to Mac-3, a macrophage marker, revealed a greater number of infiltrating macrophages (the major source of MMPs), found primarily in the aortic adventitia, in *Pik3c2a*$^{+/-}$ mice compared with wild-type mice (**Fig. 6j**).

DISCUSSION

This study shows that in endothelial cells, PI3K-C2α, a class II PI3K, has indispensable roles in sprouting angiogenesis and subsequent mural-cell recruitment and in maintaining vascular barrier integrity in quiescent vessels. C2α deficiency results in impaired angiogenesis and pathological vascular hyperpermeability with vascular damage. At the cellular level, C2α is essential for endothelial cell migration, proliferation and survival and VE-cadherin assembly at intercellular junctions. The actions of C2α are mediated by its regulatory effects on intracellular vesicular transport; that is, on the delivery and recycling of membrane molecules and on cell signaling that likely occurs on endosomes (**Supplementary Fig. 20**). These actions of C2α underlie its roles in angiogenesis and barrier integrity. The actions of C2α and of class I PI3Ks in endothelial cells are distinct: in contrast to C2α, class I PI3Ks have a large effect on Akt stimulation and cell proliferation but are not involved in vesicular trafficking and do not affect VE-cadherin trafficking to the plasma membrane or VE-cadherin assembly at the cell-cell junction[10–13]. Therefore, these observations reveal new biological activities of C2α and underscore broader roles for PI3K family members in vascular physiology and pathophysiology.

In contrast to class I PI3Ks that generate PtdIns(3,4,5)P_3, the major product of class II and III PI3Ks is PtdIns(3)P, which accumulates mainly in endosomes[16–18,20–25]. Consistent with this, C2α in endothelial cells was localized in endosomes and the TGN, organelles that are responsible for the processing, sorting and packaging of proteins for transport to their final destinations. Another class II PI3K, PI3K-C2β, and the class III PI3K Vps34 are also localized primarily in the clathrin-coated or endocytic compartment[38,39]. Localized production of PtdIns(3)P in conjunction with the presence of Rab GTPases, such as Rab5, on the endocytic membrane cause the recruitment of proteins such as EEA1 and rabenosyn-5; this recruitment facilitates dynamic formation of endocytic membranous structures for uptake, packaging and sorting[31,32,39]. Our results show that C2α is the PI3K isoform in endothelial cells that is largely responsible for PtdIns(3)P accumulation on endosomes. C2α seems to have a functionally distinct role from that of C2β or Vps34, as depletion of C2α, but not Vps34 or C2β, severely impairs trafficking of 2 × FYVE$^+$ vesicles and transport and assembly of VE-cadherin, and C2α deficiency impairs receptor internalization and VE-cadherin trafficking. Thus, C2α in endothelial cells may be located in a different endocytic compartment compared to C2β and Vps34 cells, or C2α activity may be regulated differently compared to the activities of C2β and Vps34 (refs. 18,23,40). Therefore, C2α has specialized functions in vesicular trafficking in endothelial cells.

Our data also show that C2α is involved in cell signaling. Endocytosis has long been recognized as a mechanism for terminating signaling by internalizing and degrading cell-surface receptors[41]. Besides this classical role of endocytosis, recent studies[32,41–43] have shown that endosomes serve as platforms to assemble membrane receptors and their downstream signaling molecules and to generate spatially localized signals. In endothelial cells, activation of RhoA, Rac1 and Rap1, but not of Akt or ERK, is dependent on C2α to varying degrees, indicating that the generation of certain intracellular signals requires C2α. In particular, C2α is essential for the internalization of activated VEGFR2 and endosomal RhoA activation. Consistent with the role of endosomes in receptor signaling, blockade of endocytosis suppressed VEGF-A–induced RhoA activation. Localized activation of RhoA was recently shown to be necessary for the proper assembly of VE-cadherin at intercellular junctions and for barrier-protective activity[44,45], although there is also evidence for an opposite barrier-disruptive activity of RhoA[4,46,47]. Our data indicate that C2α-dependent RhoA activity on endosomes is crucial for the delivery and assembly of VE-cadherin at cell contacts and for cell-cell contact formation. The identity of the Rho-guanine nucleotide exchange factor (Rho-GEF) that is responsible for VEGF-induced endosomal RhoA activation in endothelial cells, as well as the molecular mechanisms involved in the recruitment and activation of this factor, remain to be determined. Rap1 and Rac1 have also been implicated in strengthening VE-cadherin–mediated intercellular junctions[4,46,48].

The effects of C2α on endosomal transport and signaling may have a pivotal role in endothelial cell migration, proliferation and survival and vascular morphogenesis. For example, Rho and Rac are activated at the rear and front ends, respectively, of migrating cells to drive machinery responsible for retracting the rear portion of the cell body and extending protrusions forward[49]. During cell migration, there is assembly and disassembly of focal adhesions, which depends on endocytic and recycling vesicular functions[49,50]. Rho GTPases are involved in the formation of focal adhesions, which generate cell-survival signals through mechanisms involving integrin ligation. Polarization of the endothelial cell monolayer in the vascular wall also depends on membrane trafficking[51]. Endosomes could be involved in these processes, both by serving as a platform for the activation of Rho GTPases and recruiting Rho GTPases to specific sites within cells[45]. Taken together, our observations strongly suggest that C2α has a role in angiogenesis and vascular integrity through its regulation of vesicular trafficking.

In adult mice, C2α expression is generally diminished compared with its expression in embryos, but it is still expressed at an easily detectable level in the vascular endothelium among other tissues[19]. Our data show that C2α is essential for maintaining barrier integrity in quiescent vessels, as evidenced by its protective role in diminishing VEGF-A–induced hyperpermeability. In anaphylaxis, a 50% reduction in C2α expression markedly increased mortality. In chronic vascular injury induced by Ang II infusion, disruption of the vascular wall probably caused by disassembly of VE-cadherin in the endothelium occurs, leading to fatal dissecting aneurysm formation. Collectively, our data are consistent with the notion that a normal level of C2α expression is essential for the maintenance of vascular integrity in quiescent vasculature, as well as for neovesssel formation. These observations point to the possibility that C2α may be a new therapeutic target for vascular diseases caused by barrier disruption.

METHODS

Methods and any associated references are available in the online version of the paper.

Note: Supplementary information is available in the online version of the paper.

ACKNOWLEDGMENTS

We thank K. Mitsumori for comments on the histological study. We thank N. Mochizuki and K. Ando for assistance with the FRET imaging analysis. We thank N. Furusawa, K. Sunagawa and E. Kaneko for assistance with live-cell imaging using a Yokogawa confocal microscope system. We also thank Y. Ohta and T. Murakawa for technical assistance and T. Hirose for administrative assistance. C2α complementary DNA was obtained from J. Domin (Imperial College London). GFP-2 × FYVE and mRFP-2 × FYVE expression vectors were obtained from H. Stenmark (Oslo University Hospital) and Y. Ohsumi (Tokyo Institute of Technology), respectively. VE-cadherin-GFP expression vectors were obtained from N. Mochizuki (National Cerebral and Cardiovascular Center). The pRaichu-RhoA probe was obtained from M. Matsuda (Kyoto University). GFP-RhoA^{Asn19} and GFP-RhoA^{Val14} expression vectors were obtained from F. Valderrama (King's College London). This work was supported in part by grants-in-aid from the Japanese Ministry of Education, Culture, Sports, Science and Technology, the Japan Society for the Promotion of Science (to K. Yoshioka, N. Takuwa, Y.O. and Y.T.), the Honjin Foundation, the Mitsubishi Pharma Research Foundation and the SENSIN Medical Research Foundation (to K. Yoshioka).

AUTHOR CONTRIBUTIONS

K. Yoshioka designed the experiments, performed characterization of the developmental and retinal angiogenesis of the conditional knockout mice and most of the *in vitro* studies and analyzed the data with assistance from N. Takuwa, Y.O., W.D., S.A., H.M., C.N., K.B., M.U., N. Takakura and O.M. K.A. and T.S. analyzed the cellular content of phosphoinositides. K. Yoshida performed *in vivo* angiogenenesis experiments with K. Yoshioka, performed tumor implantation and aneurysm experiments and interpreted the results. H.C. performed the anaphylaxis experiments. W.D. performed the *in vivo* permeability study. X.Q. and Y.O. performed and interpreted the results of the ischemic angiogenesis model. T.W. and S.I. performed and interpreted the results of electron microscopy. K.S., M.A., N. Takuwa, R.J.S., H.O. and R.H.A. generated mouse mutants. K. Yoshioka and Y.T. planned and supervised the experiments, arranged the figures and wrote the manuscript. M.A. and N. Takuwa participated in writing the manuscript (M.A. wrote part of the Online Methods, and N. Takuwa wrote the Abstract, Introduction and Results sections).

COMPETING FINANCIAL INTERESTS

The authors declare no competing financial interests.

Published online at http://www.nature.com/doifinder/10.1038/nm.2928.
Reprints and permissions information is available online at http://www.nature.com/reprints/index.html.

1. Adams, R.H. & Alitalo, K. Molecular regulation of angiogenesis and lymphangiogenesis. *Nat. Rev. Mol. Cell Biol.* **8**, 464–478 (2007).
2. Coultas, L. *et al.* Endothelial cells and VEGF in vascular development. *Nature* **438**, 937–945 (2005).
3. Andrae, J. *et al.* Role of platelet-derived growth factor in physiology and medicine. *Genes Dev.* **22**, 1276–1312 (2008).
4. Mehta, D. & Malik, A.B. Signaling mechanisms regulating endothelial permeability. *Physiol. Rev.* **86**, 279–367 (2006).
5. Dejana, E., Tournier-Lasserve, E. & Weinstein, B.M. The control of vascular integrity by endothelial cell junctions: molecular basis and pathological implications. *Dev. Cell* **16**, 209–221 (2009).
6. Yoshimura, K. *et al.* Regression of abdominal aortic aneurysm by inhibition of c-Jun N-terminal kinase. *Nat. Med.* **11**, 1330–1338 (2005).
7. Satoh, K. *et al.* Cyclophilin A enhances vascular oxidative stress and the development of angiotensin II–induced aortic aneurysms. *Nat. Med.* **15**, 649–656 (2009).
8. Ferrara, N. & Kerbel, R.S. Angiogenesis as a therapeutic target. *Nature* **438**, 967–974 (2005).
9. Carmeliet, P. Angiogenesis in life, disease and medicine. *Nature* **438**, 932–936 (2005).
10. Engelman, J.A. *et al.* The evolution of phosphatidylinositol 3-kinases as regulator of growth and metabolism. *Nat. Rev. Genet.* **7**, 606–619 (2006).
11. Takenawa, T. & Suetsugu, S. The WASP-WAVE protein network: connecting the membrane to the cytoskeleton. *Nat. Rev. Mol. Cell Biol.* **8**, 37–48 (2007).
12. Vanhaesebroeck, B. *et al.* The emerging mechanisms of isoform-specific PI3K signaling. *Nat. Rev. Mol. Cell Biol.* **11**, 329–341 (2010).
13. Graupera, M. *et al.* Angiogenesis selectively requires the p110α isoform of PI3K to control endothelial cell migration. *Nature* **453**, 662–666 (2008).
14. Yuan, T.L. & Cantley, L.C. PI3K pathway alterations in cancer: variations on a theme. *Oncogene* **27**, 5497–5510 (2008).
15. Funderburk, S.F. *et al.* The Beclin 1–Vps34 complex at the crossroads of autophagy and beyond. *Trends Cell Biol.* **20**, 355–362 (2010).
16. Falasca, M. *et al.* The role of phosphoinositide 3-kinase C2α in insulin signaling. *J. Biol. Chem.* **282**, 28226–28236 (2007).
17. Linassier, C. *et al.* Molecular cloning and biochemical characterization of a *Drosophila* phosphatidylinositol-specific phosphoinositide 3-kinase. *Biochem. J.* **321**, 849–856 (1997).
18. Domin, J. *et al.* The class II phosphoinositide 3-kinase PI3K–C2α is concentrated in the trans-Golgi network and present in clathrin-coated vesicles. *J. Biol. Chem.* **275**, 11943–11950 (2000).
19. El Sheikh, S.S. *et al.* Topographical expression of class IA and class II phosphoinositide 3-kinase enzymes in normal human tissues is consistent with a role in differentiation. *BMC Clin. Pathol.* **3**, 4 (2003).
20. Yoshioka, K. *et al.* Ca^{2+}-induced, Rho- and Rho kinase-dependent regulation of myosin phosphatase and contraction in isolated vascular smooth muscle cells. *Mol. Pharmacol.* **71**, 912–920 (2007).
21. Traer, C.J. *et al.* Are class II phosphoinositide 3-kinases potential targets for anticancer therapies? *Bull. Cancer* **93**, E53–E58 (2006).
22. Gaidarov, I. *et al.* Individual phosphoinositide 3-kinase C2α domain activities independently regulate clathrin function. *J. Biol. Chem.* **280**, 40766–40772 (2005).
23. Falasca, M. & Maffucci, T. Role of class II phosphoinositide 3-kinase in cell signalling. *Biochem. Soc. Trans.* **35**, 211–214 (2007).
24. Wang, Y. *et al.* Class II phosphoinositide 3-kinase α-isoform regulates Rho, myosin phosphatase and contraction in vascular smooth muscle. *Biochem. J.* **394**, 581–592 (2006).
25. Harris, D.P. *et al.* Requirement for class II phosphoinositide 3-kinase C2α in maintenance of glomerular structure and function. *Mol. Cell. Biol.* **31**, 63–80 (2011).
26. Moses, K.A. *et al.* Embryonic expression of an Nkx2–5/Cre gene using ROSA26 reporter mice. *Genesis* **31**, 176–180 (2001).
27. Kisanuki, Y.Y. *et al.* Tie2-Cre transgenic mice: a new model for endothelial cell-lineage analysis *in vivo*. *Dev. Biol.* **230**, 230–242 (2001).
28. Wang, Y. *et al.* Ephrin-B2 controls VEGF-induced angiogenesis and lymphangiogenesis. *Nature* **465**, 483–486 (2010).
29. Pannekoek, W.J. *et al.* Cell-cell junction formation: the role of Rap1 and Rap1 guanine nucleotide exchange factors. *Biochim. Biophys. Acta* **1788**, 790–796 (2009).
30. Gillooly, D.J. *et al.* Localization of phosphatidylinositol 3-phosphate in yeast and mammalian cells. *EMBO J.* **19**, 4577–4588 (2000).
31. Lindmo, K. & Stenmark, H. Regulation of membrane traffic by phosphoinositide 3-kinase. *J. Cell Sci.* **119**, 605–614 (2006).
32. Di Paolo, G. & De Camilli, P. Phosphoinositides in cell regulation and membrane dynamics. *Nature* **443**, 651–657 (2006).
33. Bryan, B.A. *et al.* RhoA/ROCK signaling is essential for multiple aspects of VEGF-mediated angiogenesis. *FASEB J.* **24**, 3186–3196 (2010).
34. Macia, E. *et al.* Dynasore, a cell-permeable inhibitor of dynamin. *Dev. Cell* **10**, 839–850 (2006).
35. Cauwels, A. *et al.* Anaphylactic shock depends on PI3K and eNOS-derived NO. *J. Clin. Invest.* **116**, 2244–2251 (2006).
36. Daugherty, A. & Cassis, L.A. Mouse models of abdominal aortic aneurysms. *Arterioscler. Thromb. Vasc. Biol.* **24**, 429–434 (2004).
37. Di Gennaro, A. *et al.* Increased expression of leukotriene C4 synthase and predominant formation of cysteinyl-leukotrienes in human abdominal aortic aneurysm. *Proc. Natl. Acad. Sci. USA* **107**, 21093–21097 (2010).
38. Wheeler, M. & Domin, J. The N-terminus of phosphoinositide 3-kinase–C2β regulates lipid kinase activity and binding to clathrin. *J. Cell. Physiol.* **206**, 586–593 (2006).
39. Simonsen, A. & Tooze, S.A. Coordination of membrane events during autophagy by multiple class III PI3-kinase complexes. *J. Cell Biol.* **186**, 773–782 (2009).
40. Johnson, E.E. *et al.* Gene silencing reveals a specific function of hVps34 phosphatidylinositol 3-kinase in late versus early endosomes. *J. Cell Sci.* **119**, 1219–1232 (2006).
41. Doherty, G.J. & McMahon, H.T. Mechanisms of endocytosis. *Annu. Rev. Biochem.* **78**, 31.1–31.46 (2009).
42. Zoncu, R. *et al.* A phosphoinositide switch controls the maturation and signaling properties of APPL endosomes. *Cell* **136**, 1110–1121 (2009).
43. Palamidessi, A. *et al.* Endocytic trafficking of Rac is required for the spatial restriction of signaling in cell migration. *Cell* **134**, 135–147 (2008).
44. van Nieuw Amerongen, G.P. *et al.* Involvement of Rho kinase in endothelial barrier maintenance. *Arterioscler. Thromb. Vasc. Biol.* **27**, 2332–2339 (2007).
45. Yamada, S. & Nelson, W.J. Localized zones of Rho and Rac activities drive initiation and expansion of epithelial cell-cell adhesion. *J. Cell Biol.* **178**, 517–527 (2007).
46. Harris, T.J.C. & Tepass, U. Adherens junctions: from molecules to morphogenesis. *Nat. Rev. Mol. Cell Biol.* **11**, 502–514 (2010).
47. Abraham, S. *et al.* VE-cadherin–mediated cell-cell interaction suppresses sprouting via signaling to MLC2 phosphorylation. *Curr. Biol.* **19**, 668–674 (2009).
48. Noda, K. *et al.* Vascular endothelial-cadherin stabilizes at cell-cell junctions by anchoring to circumferential actin bundles through α- and β-catenins in cyclic AMP-Epac-Rap1 signal-activated endothelial cells. *Mol. Biol. Cell* **21**, 584–596 (2010).
49. Webb, D.J., Parsons, J.T. & Horwits, A.F. Adhesion assembly, disassembly and turnover in migrating cells—over and over and over again. *Nat. Cell Biol.* **4**, E97–E100 (2002).
50. Mitra, S.K., Hanson, D.A. & Schlaepfer, D.D. Focal adhesion kinase: in command and control of cell motility. *Nat. Rev. Mol. Cell Biol* **6**, 56–68 (2005).
51. Shivas, J.M. *et al.* Polarity and endocytosis: reciprocal regulation. *Trends Cell Biol.* **20**, 445–452 (2010).

ONLINE METHODS

Mice. All mice used in this study were bred and maintained at the Institute for Experimental Animals, Advanced Science Research Center, Kanazawa University under specific pathogen-free conditions. All procedures were conducted in accordance with the Fundamental Guidelines for Proper Conduct of Animal Experiment and Related Activities in Academic Research Institutions under the jurisdiction of the Ministry of Education, Culture, Sports, Science and Technology of Japan and approved by the Committee on Animal Experimentation of Kanazawa University.

A gene-targeting strategy to generate global *Pik3c2a*-null mice is described in the **Supplementary Methods**. Four lines of *Cre* mice, *Tie2*-Cre (ref. 27), *SM22a*-Cre (B6.129S6-*Tagln*$^{tm2(Cre)Yec}$/J, Jackson Lab), *Nkx2-5*-Cre (ref. 26) and tamoxifen-inducible endothelial-cell-specific *Cdh5*(PAC)-CreER^{T2} (refs. 28,52,53), were bred with *Pik3c2a*$^{flox/+}$ or *Pik3c2a*$^{flox/flox}$ mice to generate *Pik3c2a*$^{\Delta EC}$ (*Pik3c2a*$^{flox/flox}$; *Tie2*-Cre), *Pik3c2a*$^{\Delta SMC}$ (*Pik3c2a*$^{flox/flox}$; *SM22a*-Cre), *Pik3c2a*$^{\Delta MC}$ (*Pik3c2a*$^{flox/flox}$; *Nkx2-5*-Cre) and *Pik3c2a*$^{i\Delta EC}$ (*Pik3c2a*$^{flox/flox}$; *Cdh5*(PAC)-CreER^{T2}) mice, respectively. Cre-negative littermates were used as controls. To verify the efficiency of Cre recombination, Cre mice were mated with mice from the *Cre* reporter transgenic line *ROSA26*-LacZ (B6.129S4-*Gt(ROSA)26Sor*^{tm1Sor}/J, Jackson Lab). All mice had a C57BL/6J genetic background. Gene inactivation in pups was triggered by i.p. injection of 50 µl of tamoxifen solution (Sigma, T5648; 10 mg ml^{-1} corn oil) once at P3 or P6. The phenotypes of the mutant mice were analyzed at P6 or P9, as indicated. For adult mice, tamoxifen was administered by i.p. injection of 100 µl of a 10 mg ml^{-1} tamoxifen stock solution (that is, 1 mg per injection) a total of seven times, every second day.

Cell culture and siRNA knockdown. Mouse embryonic fibroblasts (MEF) and MASM were isolated from *Pik3c2a*$^{flox/flox}$ mice and used for *in vitro* assays. *Pik3c2a*$^{flox/flox}$ MEF and MASM cells were cultured in DMEM (WAKO) and advanced DMEM (Invitrogen) supplemented with 10% FBS, respectively. The cells were cultured to 70% confluency and then were infected with adenovirus encoding Cre recombinase (AdCre) in the absence of serum. Infection with adenovirus encoding LacZ (AdLacZ) was used as control. After 1 h, culture medium containing 10% FBS was added, and the cells were allowed to recover for the next 48 h. Greater than 90% C2α deletion was confirmed by western blotting (**Supplementary Fig. 13d**). HUVEC (passage 2–4) (Lonza) were grown in endothelial basal medium supplemented with 2% FBS and growth factor supplement cocktail (complete growth medium) (EBM2, Lonza, CC-3162). HUVEC were transfected with 20 nM of siRNA using Lipofectamine 2000 (Invitrogen) in OptiMEM (2 µl ml^{-1}; Gibco) according to the manufacturer's instructions. After 4 h, the culture medium was replaced with complete growth medium. The cells were cultured for a further 48–72 h before processing for immunofluorescence staining and other assays. The target sequences of the siRNA used are listed in the **Supplementary Methods**.

Whole-mount staining and immunofluorescence staining. For tissue immunohistochemistry, 4% paraformaldehyde (PFA)-fixed, paraffin-embedded tissue sections were stained using standard methods. Frozen sections were prepared by cryoprotecting fixed tissue in 20% sucrose overnight at 4 °C, snap freezing the tissue in optimal cutting temperature compound (Tissue Tek) and sectioning the tissue with a Sakura Tissue-Tek Cryo$_3$ Cryostat. Sections (7–30 µm) were washed in Ca^{2+}- and Mg^{2+}-free Dulbecco's PBS and incubated with primary antibodies diluted in the antibody dilution solution (Can Get Signal, Toyobo) overnight at 4 °C or for 2 h at room temperature. Sections were then washed in PBS with 0.1% Triton X-100 and incubated with Alexa Flour–conjugated secondary antibodies for 1 h at room temperature. The antibodies used are listed in the **Supplementary Methods**. Whole-mount immunostaining of CD31 was performed using the labeled streptavidin biotin method, as described previously[54]. Alternatively, skin from the embryo head region, flat-mount retinas from postnatal mice (P6 or P9) and en face preparations of mouse aorta were used for whole-mount immunostaining, as described previously[55] with minor modifications. PFA-fixed tissues were permeabilized with methanol when necessary. Samples were incubated in blocking buffer (1% BSA and 0.3% Triton X-100 in PBS) for 2 h and washed three times in Pblec buffer (1% Triton X-100, 1 mM $CaCl_2$, 1 mM $MgCl_2$ and 1 mM $MnCl_2$ in PBS, pH 6.8). For immunofluorescence staning, samples were incubated overnight at 4 °C with gentle rocking with antibodies to biotinylated isolectin B4 (Vector B-1205, 1:50), CD31 (1:100, BD, 557355), FITC-conjugated α-SMA (1:100, Sigma, A2647), NG2 (1:100, Chemicon, ab5320) or biotinylated VE-cadherin (1:100, eBoscience 13-1441); the antibodies were diluted in Pblec buffer (1% Triton X-100, 1 mM $CaCl_2$, 1 mM $MgCl_2$ and 1 mM $MnCl_2$ in PBS, pH 6.8). For detection using secondary antibodies, Alexa Fluor-594–conjugated streptavidin (1:200, Molecular Probe, S-11227) or Alexa Fluor-488–conjugated species-specific IgG antibodies (1:500, Molecular Probe; anti-mouse IgG (H+L), A11001; anti-rabbit IgG (H+L), A11008; anti-rat IgG (H+L), A11006) diluted in blocking buffer were applied overnight at 4 °C. The vascular area in skin or retina, number of branch points and filopodial bursts in arterial zones per unit area in flat-mount retina were measured or counted from randomly defined 15–20 microscopic fields from 5–8 retinas per group for each genotype. CD31-positive vascular areas in skin and retinas were quantified using ImageJ software. Values were normalized with field sizes.

For immunofluorescence cell staining, cells were cultured on collagen-I (Type I-P, Nitta Gelatin)-coated glass-bottom dishes or Lab-Tek chamber slides in a complete growth medium (see below) and allowed to adhere overnight. The cells were rinsed with prewarmed Ca^{2+}- and Mg^{2+}-containing PBS once and fixed in prewarmed 4% fresh PFA or PBS for 15 min, washed in PBS and then permeabilized in 0.2% Triton X-100 in PBS for 5 min when necessary. The cells were incubated with blocking reagent (DAKO, X0909) for 10 min to inhibit nonspecific protein binding. For some experiments, the cells were alternatively fixed and permeabilized by immersion in acetone or methanol at −20 °C for 10 min. After blocking, cells were incubated with primary antibodies for 2 h at room temperature or overnight at 4 °C or with Alexa Fluor-594–conjugated phalloidin (1:200, Molecular Probe, A-12381). The cells were then incubated for 1 h with goat Alexa Flour-488–(1:1,1000, Molecular Probe, A-11029) or -594–conjugated secondary antibodies (1:1,000, Molecular Probe, A-11032) in PBS. For immunostaining of active GTP-RhoA, HUVEC were serum starved in M199 medium including 0.5% fatty-acid–free BSA overnight and were stimulated with VEGF-A_{165} (30 ng ml^{-1}, PeproTech) or EBM2 complete growth medium for 30 min; the cells were then stained with antibody specific for active RhoA (GTP-RhoA; NewEast Biosciences, 26904, 1:400) (this antibody was generated using GTPγS-bound RhoA antigen) and Alexa Fluor-594–conjugated phalloidin (for F-actin staining) as described above. Where appropriate, cells were counterstained with DAPI (Molecular Probe, 300 nM) for 5 min. The cells were mounted on Prolong Gold (Molecular Probe) as an antiphotobleaching agent and examined using an inverted fluorescence microscope (Olympus IX70) under a PlanApo ×40/NA0.95 objective or a confocal laser-scanning microscope (Zeiss Axiovert 200M with LSM5 Pascal) equipped with a PlanApo ×63/NA1.4 oil-immersion objective. For quantification, the positive area in stained images was calculated using ImageJ software. Quantification was carried out for at least three independent experiments with >50 cells per experiment. Adobe Photoshop was used to adjust image levels and process image overlays.

Detection of LacZ by X-gal staining and immunostaining. For 5-bromo-4-chloro-3-indolyl-β-D-galactoside (X-gal) staining, whole embryos or tissues were dissected from E16.5–E18.5 embryos, fixed in X-gal fixative solution (0.25% glutaraldehyde, 5 mM ethylene glycol tetraacetic acid (EGTA) and 2 mM $MgCl_2$ in PBS) at room temperature for 30 min and then washed in wash buffer (2 mM $MgCl_2$ and 0.02% NP-40 in PBS) for 10 min (three times). Samples were stained in X-gal staining solution (1 mg ml^{-1} X-gal, 5 mM potassium ferricyanide and 5 mM potassium ferrocyanide in wash buffer) at 37 °C until the desired staining level was achieved. Alternatively, LacZ-specific antibody (1:400, MP Cappel, 59761) was used for multicolor immunofluorescence staining, as described previously[56]. Samples were imaged on a Leica MZ16F stereomicroscope (whole-mount tissue) or a Zeiss Axiovert 200M microscopy with a LSM5 Pascal confocal laser-scanning unit using Image Browser software (Carl Zeiss).

Postnatal retinal angiogenesis model. Eyes were dissected from neonatal mice (mutants or their respective control littermates) and fixed in 4% PFA for 2 h at room temperature. Flat-mount isolectin B4 staining of retinas was performed as described in the 'whole-mount staining' section above. The spreading of the retinal vasculature along the vitreal surface was quantified by flat mounting the retina and analysis using ImageJ software. The number of branch points and

filopodial bursts in arterial zones per unit area in the flat-mount retina was counted from 15–20 randomly defined microscopic fields from 5–8 retinas per group for each genotype. The values were normalized by field size. For labeling of proliferating cells in the retina, 300 μg of BrdU (BD) in 100 μl PBS per pup was i.p. injected 2 h before euthanasia. After isolectin B4 staining, retinas were stained with BrdU-specific antibody (1:100, BD, 555627).

Postischemic hindlimb angiogenesis model. Male *Pik3c2a*$^{i\Delta EC}$ mice and control *Pik3c2a*$^{flox/flox}$ littermates (C57BL/6 background) were subjected to surgical procedures to achieve unilateral hindlimb ischemia, as described previously[57]. In brief, the femoral artery was exposed and ligated with 8-0 silk, and the whole length of the femoral artery was excised. The blood flow of the ischemic (left) and contralateral nonischemic (right) hindlimbs was measured with a laser Doppler blood flow (LDBF) analyzer (Moor Instruments) before and after operation. The stored data were analyzed to quantify the mean LDBF per unit of two-dimensional area on the en face image of each entire hindlimb in mice in the supine position, which was determined using software provided by the manufacturer (Moor Instruments). For each mouse, results were expressed as the ratio of the LDBF value in the ischemic (left) limb to the value in the nonischemic control (right) limb at a given time point.

Tumor angiogenesis model. LLC cells (1×10^6) or B16-BL6 melanoma cells (5×10^5) were subcutaneously implanted in the dorsal backs of 8- to 10-week-old male *Pik3c2a*$^{i\Delta EC}$ mice and control *Pik3c2a*$^{flox/flox}$ littermates (C57BL/6 background)[58]. Tumor volumes were calculated by the formula $V = (LW^2)/2$, where L and W denote the longer and shorter diameter, respectively.

PAF-induced anaphylaxis model. To trigger anaphylactic shock, 10- to 12-week-old male *Pik3c2a*$^{+/-}$ or littermate wild-type mice received i.v. injection of PAF (12 μg per kg body weight or 20 μg per kg body weight in 100 μl saline) in the tail vein, and their survival was followed. In separate mice, 15 min after infusion, blood samples were obtained from the right ventricle to determine hematocrit content. To assess vascular leakage in the lung, 100 μl of a 1% solution of Evans blue dye in saline was injected into the tail vein together with PAF. Fifteen minutes later, mice were perfused with saline in the right ventricle to remove the intravascular Evans blue dye. The lungs were excised and extracted in 1 ml of formamide at 55 °C overnight. Evans blue content was determined by the equation: corrected 620-nm optical density (OD_{620} (Evans blue) − (1.426 × OD_{740} (hemoglobin) + 0.03).

Ang II infusion aortic aneurysm model. An osmotic minipump (Alzet, model 1002) containing Ang II (Calbiochem, 1.0 mg per kg body weight per day) was implanted in the midscapular region in male *Pik3c2a*$^{+/-}$ or *Pik3c2a*$^{i\Delta EC}$ and wild-type littermates. Mice were euthanized at day 14 after minipump implantation, and aortic tissue was removed. Aneurysm severity was graded according to the following criteria[59]: grade 1, remodeled tissue in the suprarenal region frequently containing thrombus; grade 2, pronounced bulbous form of grade 1 containing thrombus; grade 3, multiple aneurysms containing thrombus; or ruptured, ruptured aortic aneurysm. Both cryostat and paraffin-embedded aortic sections were used for the characterization of aneurysmal lesions. Elastin was visualized using Elastica van Gieson staining. Fibrosis was evaluated using Azan staining. Infiltrating macrophages were detected using Mac-3–specific antibody (1:400, BD, 553322) immunostaining. Miles assay and gelatin zymography were performed as described below.

Live-cell imaging and FRET analysis. Cells transfected with expression vectors for GFP-C2α, GFP- or mRFP-2 × FYVE and VE-cadherin–GFP or –mRFP were plated on collagen-coated glass-bottomed dishes (MatTek, P35G-1.5-20-C) or LabTek chamber slides (Thermo Scientific, 177402) and allowed to adhere for 16 h before imaging. Cells on a heated stage (37 °C; Tokai-Hit) were observed under a custom confocal microscope based on an inverted IX70 microscope (Olympus) equipped with an UPLSAPO ×60/NA1.35-oil or ×40/0.95-oil objective, a confocal laser unit (CSU10, Yokogawa), an electron multiplying charge-coupled device (EMCCD) digital camera (iXon, Andor) and a Light engine (Lumencor, Inc) for three-dimensional time-lapse confocal imaging at a rate of two frames per second. The acquisition and process were controlled by iQ software (Andor).

For FRET analysis, HUVEC were transfected with the pRaichu-RhoA FRET probe vector (provided by M. Matsuda at Kyoto University) using an Amaxa Nucleofector system (Lonza) and imaged using a custom confocal microscope system configured with a CFP and YFP filter set (Di01-T445/515/561-13 × 15 × 0.5, Semrock). Pseudograyscale ratio images were generated from images from the CFP and FRET channels using Andor iQ software.

Cell proliferation, migration, adhesion, apoptosis and tube-formation assay. Cell proliferation was analyzed using an MTS (3-(4,5-dimethylthiazol-2-yl)-5-(3-carboxymethoxyphenyl)-2-(4-sulfophenyl)-2H-tetrazolium, inner salt) assay kit (Promega) according to the manufacturer's instructions. For the modified Boyden chamber cell migration assay, siRNA-transfected HUVEC (5×10^4 cells per well) resuspended in M199 medium (Gibco) containing 0.25% fatty-acid–free BSA (Sigma-Aldrich) or adenovirus-infected MASM cells (2×10^4 cells per well) resuspended in serum-free DMEM were placed in the upper chamber and allowed to migrate across collagen type I–coated polycarbonate filters (8-μm pore size, Neuro Probe) for 6 h toward the lower chamber with or without VEGF-A (0.5–100 ng ml^{-1}) for HUVEC and with or without PDGF-BB (0.1–30 ng ml^{-1}) for MASM. The cells remaining on the upper surface of the transwell membranes were removed, and the cells that had migrated to the lower surface were methanol fixed, stained with Diff-Quick (Sysmex) and counted in five random microscopic fields. To analyze cell adhesion to a collagen-covered surface, HUVEC that had been transfected with scrambled (control) or C2α-siRNAs were seeded onto 96-well tissue culture plates coated with collagen type I and incubated in the presence of VEGF-A (30 ng ml^{-1}) for the indicated time periods. After washing with PBS three times to remove nonadherent cells, adherent cells were stained with Diff-Quick and quantified in triplicates with a microplate reader (Bio-Rad). To assay apoptosis, cells were immunostained with cleaved caspase-3–specific antibody (1:1,000, Cell Signaling, 9664) according to the manufacturer's instructions (Cell Signaling). To assay tube formation, siRNA-transfected HUVEC (2.5×10^4 cells) in EBM2 containing 2% FBS with or without supplements were seeded onto 200 μl of growth-factor–reduced Matrigel in a 24-well plate in the absence or presence of VEGF-A (30 ng ml^{-1}) and incubated for 12–16 h. Tube formation was quantified after 12–16 h by measuring the cumulative tube length and number of branching points in five random microscopic fields using ImageJ (NIH).

Pulldown assay of small G protein activity. The pulldown assays for GTP-bound RhoA, Rac1 and Rap1were performed as described previously[60]. In brief, confluent HUVEC were stimulated and lysed with either Rho extraction buffer (50 mM Tris-HCl, pH 7.5, 500 mM NaCl, 10 mM $MgCl_2$, 1% Triton X-100, 0.5% sodium deoxycholate, 0.1% SDS, 10% glycerol and protease and phosphatase inhibitor cocktail (Roche)), Rac extraction buffer (50 mM Tris-HCl, pH 7.5, 500 mM NaCl, 10 mM $MgCl_2$, 1% Triton X-100, 0.5% sodium deoxycholate, 0.1% SDS, 10% glycerol and protease inhibitor cocktail) or Rap extraction buffer (20 mM Tris-HCl, pH 7.5, 100 mM NaCl, 10 mM $MgCl_2$, 1% NP-40, 1 mM EGTA and protease inhibitor cocktail). The lysates were cleared by centrifugation, and the resultant supernatants were incubated for 60 min at 4 °C with glutathione-Sepharose 4B beads coupled to the Rho binding domain of Rhotekin for RhoA, the PAK1-CRIB domain for Rac1 or the Rap-binding domain of Ral-GDI for Rap1. The beads were washed and bound proteins were solubilized by the addition of 30 μl of SDS-PAGE 2 × Laemmli's loading buffer, followed by separation on 15% SDS-PAGE gels and western blotting with RhoA-specific (1:1,000, Santa Cruz sc-418, 26C4), Rac1-specific (1:2,000, Millipore 05-389, 23A8) and Rap1-specific (1:1,000, BD, 610195) antibodies, respectively.

***In vitro* transwell and *in vivo* Miles permeability assay.** HUVEC transfected with C2α-siRNA or sc-siRNA were seeded onto collagen-coated transwells with a 0.4-μm pore size (Costar) and allowed to form a monolayer. Permeability was stimulated with VEGF-A_{165} (50 ng ml^{-1}) or thrombin (0.5 U ml^{-1}) for 30 min, followed by the addition of FITC-dextran (at a final concentration of 1 mg ml^{-1}) (molecular mass (Mr) = 42 kDa; Sigma-Aldrich) into the top chamber followed by incubation for an additional 30 min. The amount of FITC-dextran in the bottom chamber was determined by fluorometric analysis.

To assay *in vivo* permeability, 1.0% Evans blue dye in saline (100 μl) was i.v. injected into the tail vein of *Pik3c2a*$^{+/+}$ and *Pik3c2a*$^{+/-}$ mice and allowed to

circulate for 20 min. Recombinant human VEGF-A_{165} (100 ng ml^{-1}, 100 µl; PeproTech) or PBS was injected intradermally into the preshaved back skin. After 20 min, the mice were euthanized, and the area of skin that included the entire injection site was removed. For the Ang II infusion model, 100 µl of a 1% solution of Evans blue dye in saline was injected into the tail veins of male *Pik3c2a*$^{+/-}$ mice or *Pik3c2a*$^{+/+}$ littermates that had received Ang II infusion for 14 d prior (1.0 mg per kg body weight per day). Thirty minutes later, mice were perfused with saline in the right ventricle to remove intravascular Evans blue dye, and the heart and aorta tissues were excised. Evans blue dye was extracted from the tissues by incubation with formamide overnight at 55 °C, and Evans blue content was determined spectrophotometrically as described above.

Metabolic cell labeling, lipid extraction and phosphoinositide measurements. The amounts of cellular phosphoinositides were determined as described previously[61]. In brief, MEF were labeled for 48 h with 10 µCi ml^{-1} [^{3}H]-myo-inositol (Amersham Biosciences) in inositol-free DMEM containing 10% FBS. Labeling was quenched and lipids were extracted as described[61]. Dried lipids were deacylated and analyzed by HPLC using a Partisphere SAX column (Whatman). Radioactivity was measured in 0.5 ml fractions using a liquid scintillation counter.

Statistical analyses. Unless otherwise noted, data are presented as means ± s.e.m. and were analyzed using Prism 5 software (GraphPad Software Inc). Paired data were compared by two-tailed Student's *t* test or Mann-Whitney nonparametric *U* test. Comparisons between multiple groups were analyzed by one- or two-way ANOVA followed by Bonferroni's *post-hoc* test. For the Kaplan-Meier curves, *P* values were determined with a log-rank Mantel-Cox test. Results with $P < 0.05$ were considered statistically significant. The presented data represent at least three independent experiments.

Additional methods. Additional methodology is described in the online **Supplementary Methods**.

52. Sörensen, I., Adams, R.H. & Gossler, A. Dll1-mediated Notch activation regulates endothelial identity in mouse fetal arteries. *Blood* **113**, 5680–5688 (2009).
53. Bazigou, E. *et al.* Integrin-α9 is required for fibronectin matrix assembly during lymphatic valve morphogenesis. *Dev. Cell* **17**, 175–186 (2009).
54. Takakura, N. *et al.* Critical role of the TIE2 endothelial cell receptor in the development of definitive hematopoiesis. *Immunity* **9**, 677–686 (1998).
55. Benedito, R. *et al.* The Notch ligands Dll4 and Jagged1 have opposing effects on angiogenesis. *Cell* **137**, 1124–1135 (2009).
56. Compagni, A. *et al.* Control of skeletal patterning by ephrinB1-EphB interactions. *Dev. Cell* **5**, 217–230 (2003).
57. Oyama, O. *et al.* The lysophospholipid mediator sphingosine-1-phosphate promotes angiogenesis *in vivo* in ischemic hindlimbs of mice. *Cardiovasc. Res.* **78**, 301–307 (2008).
58. Du, W. *et al.* $S1P_2$, the G protein–coupled receptor for sphingosine-1-phosphate, negatively regulates tumor angiogenesis and tumor growth *in vivo* in mice. *Cancer Res.* **70**, 772–781 (2010).
59. Deng, G.G. *et al.* Urokinase-type plasminogen activator plays a critical role in angiotensin II–induced abdominal aortic aneurysm. *Circ. Res.* **92**, 510–517 (2003).
60. Okamoto, H. *et al.* Inhibitory regulation of Rac activation, membrane ruffling, and cell migration by the G protein-coupled sphingosine-1-phosphate receptor EDG5 but not EDG1 or EDG3. *Mol. Cell. Biol.* **20**, 9247–9261 (2000).
61. Sasaki, T. *et al.* Function of PI3Kγ in thymocyte development, T cell activation, and neutrophil migration. *Science* **287**, 1040–1046 (2000).

PLOS ONE

Origins and Properties of Dental, Thymic, and Bone Marrow Mesenchymal Cells and Their Stem Cells

Yukiya Komada[1], Toshiyuki Yamane[1], Daiji Kadota[1], Kana Isono[1], Nobuyuki Takakura[2], Shin-Ichi Hayashi[3], Hidetoshi Yamazaki[1]*

1 Department of Stem Cell and Developmental Biology, Mie University Graduate School of Medicine, Tsu, Japan, **2** Department of Signal Transduction, Research Institute for Microbial Disease, Osaka University, Suita, Japan, **3** Division of Immunology, School of Life Science, Faculty of Medicine, Tottori University, Yonago, Japan

Abstract

Mesenchymal cells arise from the neural crest (NC) or mesoderm. However, it is difficult to distinguish NC-derived cells from mesoderm-derived cells. Using double-transgenic mouse systems encoding *P0-Cre*, *Wnt1-Cre*, *Mesp1-Cre*, and *Rosa26EYFP*, which enabled us to trace NC-derived or mesoderm-derived cells as YFP-expressing cells, we demonstrated for the first time that both NC-derived (P0- or Wnt1-labeled) and mesoderm-derived (Mesp1-labeled) cells contribute to the development of dental, thymic, and bone marrow (BM) mesenchyme from the fetal stage to the adult stage. Irrespective of the tissues involved, NC-derived and mesoderm-derived cells contributed mainly to perivascular cells and endothelial cells, respectively. Dental and thymic mesenchyme were composed of either NC-derived or mesoderm-derived cells, whereas half of the BM mesenchyme was composed of cells that were not derived from the NC or mesoderm. However, a colony-forming unit-fibroblast (CFU-F) assay indicated that CFU-Fs in the dental pulp, thymus, and BM were composed of NC-derived and mesoderm-derived cells. Secondary CFU-F assays were used to estimate the self-renewal potential, which showed that CFU-Fs in the teeth, thymus, and BM were entirely NC-derived cells, entirely mesoderm-derived cells, and mostly NC-derived cells, respectively. Colony formation was inhibited drastically by the addition of anti-platelet-derived growth factor receptor-β antibody, regardless of the tissue and its origin. Furthermore, dental mesenchyme expressed genes encoding critical hematopoietic factors, such as interleukin-7, stem cell factor, and cysteine-X-cysteine (CXC) chemokine ligand 12, which supports the differentiation of B lymphocytes and osteoclasts. Therefore, the mesenchymal stem cells found in these tissues had different origins, but similar properties in each organ.

Citation: Komada Y, Yamane T, Kadota D, Isono K, Takakura N, et al. (2012) Origins and Properties of Dental, Thymic, and Bone Marrow Mesenchymal Cells and Their Stem Cells. PLoS ONE 7(11): e46436. doi:10.1371/journal.pone.0046436

Editor: Pranela Rameshwar, University of Medicine and Dentistry of New Jersey, United States of America

Received June 7, 2012; **Accepted** August 29, 2012; **Published** November 21, 2012

Funding: This work was supported by Grants-in-Aid for Scientific Research (B) (no. 21390489: HY) and Challenging Exploratory Research (no. 21659422: HY) from the Japan Society for the Promotion of Science and by funding from the Molecular Medical Science Institute, Takeda Pharmaceutical Co., Ltd. (HY). The funders had no role in study design, data collection and analysis, decision to publish, or preparation of the manuscript.

Competing Interests: The authors have declared that no competing interests exist.

* E-mail: yamazaki@doc.medic.mie-u.ac.jp

Introduction

All organs consist of layers of epithelial cells derived from one of the germ layers and mesenchymal cells derived from the neural crest (NC) or mesoderm. NC cells emerge from the dorsal region of the neural tube during embryogenesis and differentiate into melanocytes, neurons, glia, and mesenchymal cells, including osteoblasts, chondrocytes, adipocytes, odontoblasts, and perivascular cells [1,2]. NC cells participate in the organogenesis of the craniofacial area, including the tooth, heart, thymus, and bone marrow (BM) [2–7]. In particular, the cephalic NC supplies perivascular cells to the craniofacial area and thymus [8–10].

Mesoderm-derived cells have the potential to differentiate into osteoblasts, chondrocytes, and adipocytes, and contribute to the mesenchymal cells in the heart, thymus, and BM [2,4,11]. The craniofacial skeleton, including the mandible and maxilla, mainly develops from NC-derived cells; the skeleton outside this region mainly develops from mesoderm-derived cells [2,12]. Some mesoderm-derived cells contribute to the bones and cartilage of the cranial base and head muscles [13,14]. Mouse neck and shoulder skeleton is derived from mesenchymal cells that develop from both mesoderm-derived and NC-derived cells [15]. However, it is difficult to distinguish between NC-derived and mesoderm-derived cells.

Mesenchymal stem cells (MSCs) are long-term self-renewing cells, giving rise to one or more specialized cell types [16]. Friedenstein et al. first identified MSCs *in vitro* and termed them fibroblastic colony-forming units (CFU-F) [17]. They defined CFU-Fs as a BM cell population grown in a serum-containing medium that produces colonies of adherent fibroblast-like cells, which can differentiate into osteoblasts, chondrocytes, and adipocytes [17]. Although the origin of MSCs is unclear, they are present in both embryonic and adult tissues in mice and humans [16,18–20]. NC-derived multipotent cells in rodents can differentiate into neurons, glia, and myofibroblasts in the gut and sciatic nerve [21–23]; they have potentials similar to MSCs in the skin and BM [6,24–26].

To distinguish NC-derived cells from mesoderm-derived cells, we used double-transgenic mouse systems encoding *P0-Cre*, *Wnt1-Cre*, *Mesp1-Cre*, and *Rosa26EYFP*, which enabled us to trace NC- or mesoderm-derived cells as YFP-expressing cells [27–32]. *Wnt1* and *P0* are expressed in early migratory NC [5,30], and *Mesp1*, a transcription factor, is first observed at E6.5 (early gastrulation

stages), specifically in nascent mesoderm-derived cells [28]. In this study, we investigated the contributions of NC-derived and mesoderm-derived cells to the teeth, thymus, and BM using three transgenic mouse lines to establish the origin and properties of dental, thymic, and BM MSCs. CFU-F assays indicated that dental, thymic, and BM CFU-Fs comprise NC-derived and mesoderm-derived cells. We clarified the presence of cells in CFU-F progeny with the capacity for repeatable colony formation and retained multipotency.

Results

Contributions of NC-derived and mesoderm-derived cells to dental mesenchyme

We used *Wnt1-Cre*, *P0-Cre*, and *Mesp1-Cre* mice crossed with *Rosa26EYFP* mice (i.e., *Wnt1/YFP*, *P0/YFP*, and *Mesp1/YFP* mice, respectively) to investigate the contribution of NC-derived and mesoderm-derived cells to dental mesenchyme. Initially, we isolated hematopoietic cell-deprived YFP$^+$ and YFP$^-$ cells and examined the gene expression associated with the NC or mesoderm. Approximately two-thirds of YFP$^+$ cells from E9.5 *Wnt1/YFP* or *P0/YFP* embryos (i.e., Wnt1/YFP$^+$ and P0/YFP$^+$ cells) expressed p75NGFR (Fig. S1A). E9.5 Wnt1/YFP$^+$ (P0/YFP$^+$) and Mesp1/YFP$^-$ cells expressed NC-associated genes such as *AP2* and *Sox10* (Fig. S1B). Wnt1/YFP$^+$ cells in the dental mesenchyme, which were isolated from E13.5 and two-day-old mice, expressed NC-associated genes such as *p75*, *Sox10*, and *Krox20*, whereas Wnt1/YFP$^-$ cells expressed *Brachyury (T)*, a mesodermal gene (Fig. S1C). Therefore, we concluded that *Wnt1-Cre* and *P0-Cre* identified NC-derived cells.

To assess the proportion of Wnt1/YFP$^+$ cells in the dental mesenchymal cells, we prepared samples from mice that were devoid of blood cells. We found that approximately 90% of dental mesenchymal cells from E13.5 or two-day-old mice were Wnt1/YFP$^+$, whereas only approximately 7% were Mesp1/YFP$^+$ (Fig. 1A). This difference of approximately 10-fold was observed despite the presence of both NC-derived and mesoderm-derived cells in dental mesenchyme. Large numbers of E13.5 or two-day-old Wnt1/YFP$^+$ cells were observed in histological sections of the dental mesenchymal layer around the enamel organ and dental pulp, and Wnt1/YFP$^+$ cells were distributed throughout the mesenchyme, whereas only small numbers of Mesp1/YFP$^+$ cells were found in these locations (Fig. 1B, C).

Characteristics of dental mesenchymal cells and the origins of their CFU-Fs

We fractionated dental mesenchymal cells using three markers to compare their origins: CD31 (an endothelial marker), platelet-derived growth factor receptor-α (PDGFRα) (a mesenchymal cell marker), and PDGFRβ (a mesenchymal cell or perivascular cell marker). Among the E13.5 dental mesenchymal cells, Mesp1/YFP$^+$ expressed CD31 but Wnt1/YFP$^+$ cells rarely expressed it. In contrast, Wnt1/YFP$^+$ cells expressed PDGFRα and PDGFRβ but Mesp1/YFP$^+$ rarely expressed these markers(Fig. 1A). *Wnt1-Cre* and *Mesp1-Cre* were indicators of reciprocally separable cell populations. PDGFRα- and PDGFRβ-expressing cells were found only in the Mesp1/YFP$^-$ cell fraction. Dental pulp cells from two-day-old and four-week-old mice produced similar results (Fig. 1A). We also examined the expression of the endothelial cell markers CD34, FLK1, and Sca1 (an MSC marker). Sca1 was expressed in Mesp1/YFP$^+$ cells from two-day-old mice (Fig. 1A). All four-week-old Mesp1/YFP$^+$ cells expressed CD31, whereas 42% and 53% expressed CD34 and FLK1, respectively (Fig. S2). Similarly, histological sections revealed that Wnt1/YFP$^+$ cells in the

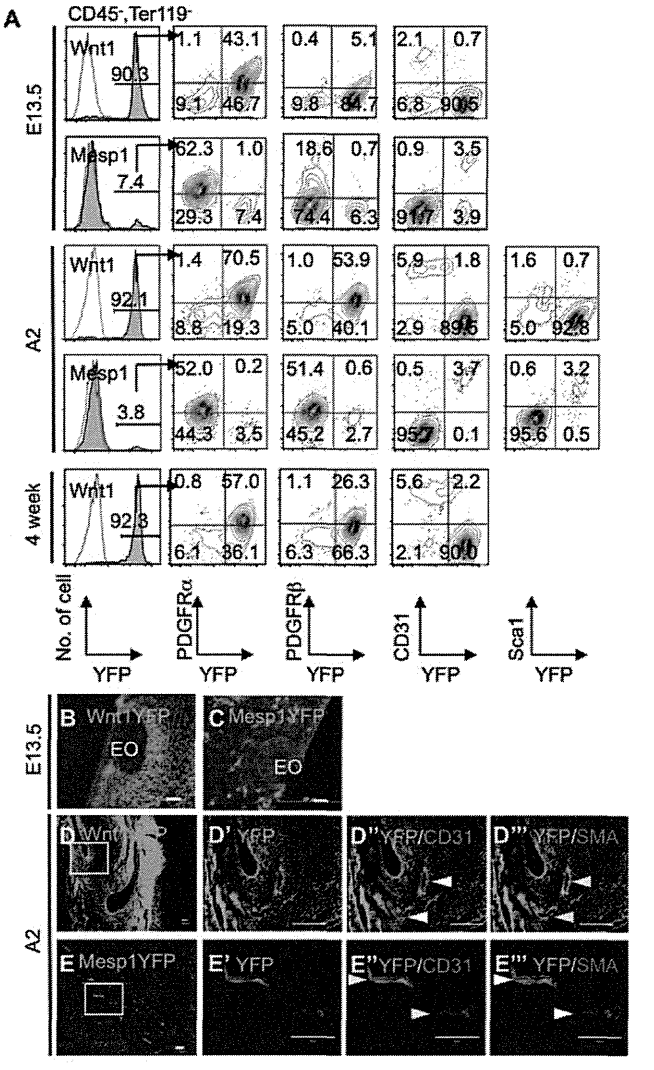

Figure 1. Origins and characteristics of NC-derived and mesoderm-derived cells of the dental mesenchyme. (A) Expression of YFP and cell surface molecules by dental mesenchymal cells prepared from E13.5, 2-day-old, and 4-week-old *Wnt1-Cre/YFP* and *Mesp1-Cre/YFP* mice. The proportions of YFP$^+$ cells in the CD45$^-$ and Ter119$^-$ fractions are indicated. (B, C) Immunohistochemistry of YFP in the mandibular molars of E13.5 *Wnt1-Cre/YFP* (B) and *Mesp1-Cre/YFP* embryos (C). EO, enamel organ. (D, E) Immunohistochemistry of YFP, CD31, and α-SMA in the mandibular incisors of 2-day-old *Wnt1-Cre/YFP* (D) and *Mesp1-Cre/YFP* mice (E). High-magnification views (D′–D‴and E′–E‴) of the boxed areas in (D) and (E), respectively. Yellow and white arrowheads indicate positive cells for each antibody to indicate the presence or absence of YFP$^+$ cells, respectively. Scale bars = 50 μm. All experiments were repeated in duplicate and one representative experiment is presented.
doi:10.1371/journal.pone.0046436.g001

perivascular lining of two-day-old mice expressed α-SMA, but not CD31 (Fig. 1D′–D‴). In 2-day-old mice, Mesp1/YFP$^+$ dental mesenchymal cells were located in the inner layer of blood vessels and expressed CD31, but not α-smooth muscle actin (α-SMA)(Fig. 1E′–E‴). Thus, NC-derived and mesoderm-derived cells may contribute to α-SMA$^+$ perivascular cells and CD31$^+$ endothelial cells, respectively.

We performed CFU-F assays to determine the origin of dental MSCs, which are functional assays for measuring MSCs *in vitro* (Fig. 2A). We used unfractionated cells, including YFP$^+$ and YFP$^-$

cells from E13.5 *Wnt1/YFP* or *Mesp1/YFP* embryos, but all colonies comprised Wnt1/YFP$^+$ or Mesp1/YFP$^-$ cells (Fig. 2B, C). Using unfractionated dental pulp cells from two-day-old mice, we found that all colonies were Wnt1/YFP$^+$, except one, and that all consisted of Mesp1/YFP$^-$ cells (Fig. 2C). Four-week-old *Mesp1/YFP* and *Wnt1/YFP* mice yielded similar results (Table S1).

To estimate the self-renewal activity of CFU-Fs, we examined the capacity for repeatable colony formation (secondary or tertiary CFU-F assays). Cells from primary colonies were used to detect secondary CFU-Fs. The frequency of secondary colony formation (0.37%–2.00%) was approximately 10 times higher than that of primary colony formation (0.06%–0.29%) (Table S1). These results suggest that dental CFU-Fs contain self-renewing MSCs. All secondary colonies were Wnt1/YFP$^+$, but only one secondary colony from four-week-old *Mesp1/YFP* mice was composed of Mesp1/YFP$^+$ cells in one of two independent experiments (Table S1, Exp. 1). The YFP$^+$ cells from *Mesp1/YFP* mice exhibited proliferative capacity. However, the frequency of Mesp1/YFP$^+$ colony formation was very low in the tertiary CFU-F assays (0.1%; 2/2,000 cells) compared with Wnt1/YFP$^+$ colonies (Fig. S3A).

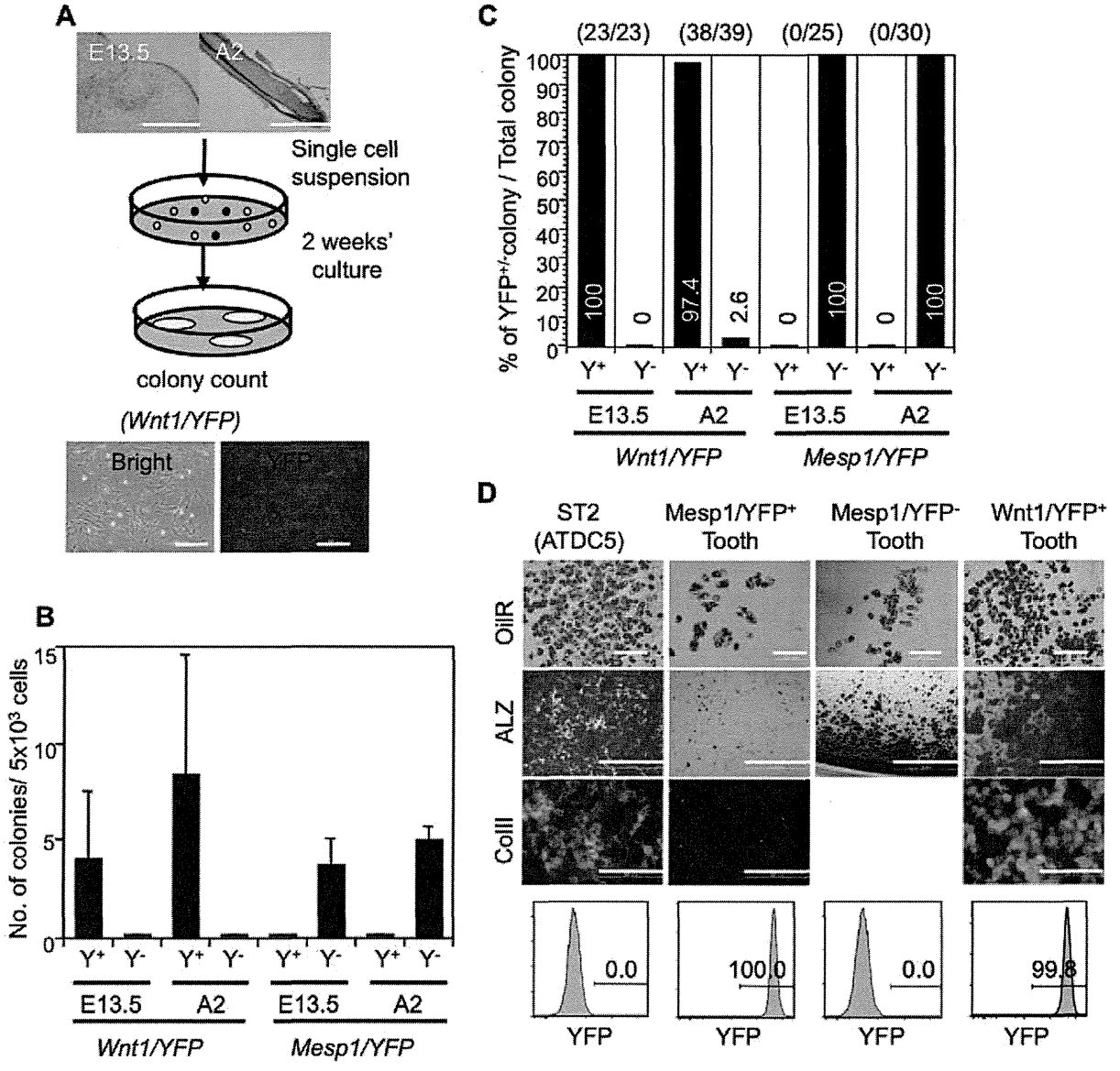

Figure 2. CFU-F assays and differential potential of dental mesenchymal cells of *Wnt1-Cre/YFP* and *Mesp1-Cre/YFP* mice. (A) Protocol of the CFU-F assays and fibroblastic colonies obtained from *Wnt1-Cre/YFP* mice. Scale bars, 200 μm. (B) Numbers of colonies induced from dental mesenchymal cells including both YFP$^+$ and YFP$^-$ cells of E13.5 and 2-day-old *Wnt1-Cre/YFP* and *Mesp1-Cre/YFP* mice. Values represent the mean (SD) of triplicate cultures of two independent experiments. Y$^+$, YFP$^+$ colonies; Y$^-$, YFP$^-$ colonies. (C) Percentages of YFP$^+$ and YFP$^-$ colonies induced from dental mesenchymal cells of *Wnt1-Cre/YFP* and *Mesp1-Cre/YFP* mice. Figures within parentheses indicate the number of YFP$^+$ colonies of the total number of colonies. Values represent percentages and colony numbers of triplicate cultures of two independent experiments ($n = 6$/group). (D) Differentiation potential of NC-derived and mesoderm-derived dental mesenchymal cells into adipocytes, osteoblasts, and chondrocytes. Cells from YFP$^+$ or YFP$^-$ colonies using dental mesenchymal cells from *Wnt1-Cre/YFP* or *Mesp1-Cre/YFP* mice were collected using a cell sorter. YFP expression in each cell preparation is shown in the lower panel. The cultured cells were stained with oil red O (OilR), alizarin red (ALZ), and anti-type II collagen (Col II) antibody to detect adipocytes, osteoblasts, and chondrocytes, respectively. ST2 and ATDC5 cells were the positive controls. The experiments were repeated twice and one representative experiment is presented. Scale bars, 200 μm in OilR and Col II and 1 mm in ALZ.
doi:10.1371/journal.pone.0046436.g002

Mesp1/YFP$^+$ cells recovered from primary or secondary colonies expressed PDGFRβ, but scarcely expressed CD31, which was similar to Wnt1/YFP$^+$ cells (Fig. S3B, C). Thus, CFU-Fs containing dental MSCs in the dental mesenchyme were generated mainly from NC-derived cells and rarely from mesoderm-derived cells.

Dental CFU-Fs with the potential for differentiation into osteoblasts, adipocytes, and chondrocytes are derived from NC

CFU-Fs are defined as cells with the potential for differentiation into osteoblasts, adipocytes, and chondrocytes *in vitro*. To assess whether colonies induced from dental mesenchymal cells could differentiate into these types, we performed CFU-F assays using two-day-old or four-week-old *Wnt1/YFP* and *Mesp1/YFP* mice. Cell suspensions prepared from YFP$^+$ colonies were cultured using reagents to induce their differentiation. Because Mesp1/YFP$^+$ dental mesenchymal cells formed few colonies in the CFU-F assays, Mesp1/YFP$^+$ cells were sorted and cultured. The cultured cells were stained with ALZ, OilR, or anti-type II collagen (Col II) antibody after 2–3 weeks to detect osteoblasts, adipocytes, and chondrocytes, respectively. Large numbers of ALZ$^+$, OilR$^+$, and Col II$^+$ cells were induced from Wnt1/YFP$^+$ dental mesenchymal cells (Fig. 2D). P0/YFP$^+$ dental mesenchymal cells also produced similar results. However, OilR$^+$ cells and a small number of ALZ$^+$ cells, but no Col II$^+$ cells, were induced from Mesp1/YFP$^+$ dental mesenchymal cells. In contrast, large numbers of ALZ$^+$ and OilR$^+$ cells were induced from Mesp1/YFP$^-$ cells (Fig. 2D). These results indicate that dental CFU-Fs with MSC properties were present in the dental pulp and were derived only from NC.

Roles of PDGFRs in CFU-Fs from dental mesenchymal cells

It is known that PDGFRs are expressed on MSCs, and PDGFRα$^+$ and PDGFRβ$^+$ cells were found among Wnt1/YFP$^+$ dental mesenchymal cells. PDGF is related to the CFU-F colony size when culturing BM cells in serum-deprived conditions [33], but the roles of PDGFRs in dental mesenchymal cells are unclear. We assessed their roles in colony formation using inhibitory antibodies against PDGFRα (anti-PDGFRα) and/or PDGFRβ (anti-PDGFRβ). We classified the colonies as either large (>50 cells) or small (approximately 8–50 cells). Anti-PDGFRα alone had little effect on colony formation, whereas anti-PDGFRβ decreased the number of large colonies to 15% of that observed in the presence of the isotype control or anti-PDGFRα in the primary CFU-F assay (Table S2, Fig. 3A). The total colony number observed in the presence of anti-PDGFRβ was 55% of that observed in the presence of anti-PDGFRα or the isotype control (Table S2, Fig. 3A). Similarly, in the secondary CFU-F assay, the number of total and large colonies formed in the presence of anti-PDGFRβ were 65% and 33%, respectively, of those observed in the presence of the isotype control (Fig. 3B). Thus, signaling by PDGFRβ is important for maintaining dental CFU-Fs. However, we cannot rule out the possibility that PDGFRβ signaling promoted the proliferation of CFU-F descendants (Fig. 3A, B), because anti-PDGFRβ affected the number of large colonies rather than the total number of colonies. To clarify this issue, we performed a primary CFU-F assay in the presence of anti-PDGFRβand/or anti-PDGFRα, and a secondary CFU-F assay in the absence of these antibodies. Cells prepared from colonies in the primary CFU-F assay treated only with anti-PDGFRβ or with both anti-PDGFRα and anti-PDGFRβ produced 50% or 0% of cells prepared from colonies observed in the presence of the

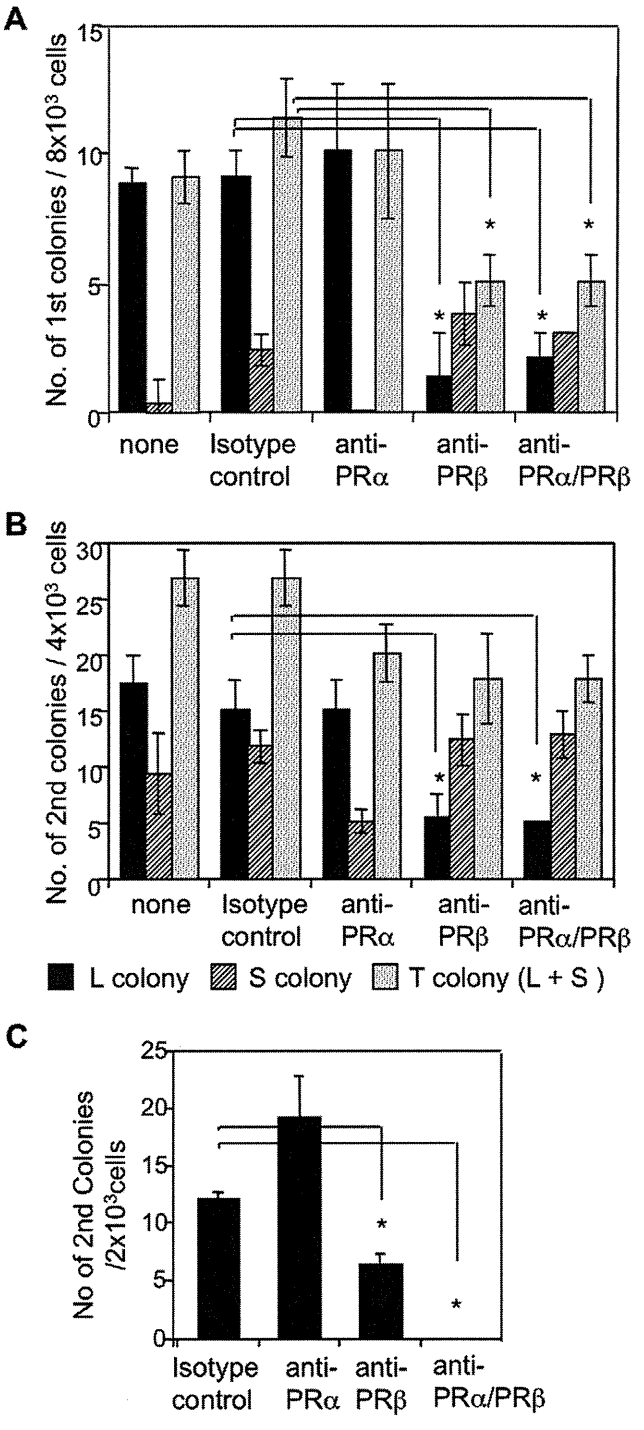

Figure 3. Effects of inhibitory antibodies against PDGFRα and/or PDGFRβ in CFU-F assays using dental mesenchymal cells. (A) Numbers of primary colonies (1st CFU-F) induced from dental mesenchymal cells from 4-week-old mice in the presence of anti-PDGFRα (APA5) and/or anti-PDGFRβ (APB5). None, no antibody. Numbers of large (L, >50 cells), small (clusters) (S, 8–50 cells), and total colonies (T, L+S colonies) are shown. (B) Numbers of secondary colonies (2nd CFU-F) induced from primary colonies of 4-week-old mice in the presence of anti-PDGFRα and/or anti-PDGFRβ. The primary CFU-F assay was performed in the absence of these antibodies. Numbers of large, small, and total colonies are shown. (C) Numbers of secondary colonies (2nd CFU-F) induced from primary colonies from 4,000 dental mesenchymal cells of 4-week-old mice in the presence of anti-PDGFRα and/or anti-PDGFRβ. The secondary CFU-F assay was performed in the

absence of antibodies. Values represent the means (SD) of triplicate cultures. Asterisks indicate a significant difference from the number of colonies in the presence of the isotype-matched control antibody ($p<0.05$). The experiments were repeated twice and one representative experiment is presented.
doi:10.1371/journal.pone.0046436.g003

isotype control in the secondary CFU-F assay (Fig. 3C). Thus, PDGFRβ signaling is important for maintaining self-renewal of dental CFU-Fs, rather than proliferation of CFU-F descendants.

Origins and characteristics of thymic and BM mesenchymal cells

Previously, we reported that multipotent NC-derived cells participate in the formation of fetal thymic and dental mesenchyme [31,32]. However, the origins and characteristics of BM and thymic mesenchymal cells and their MSCs remain unclear. Thus, we examined whether NC-derived and mesoderm-derived cells contributed to BM and thymic mesenchyme from the fetal stage to the adult stage.

In the BM, both Mesp1/YFP$^+$ and P0/YFP$^+$ (Wnt1/YFP$^+$) cells contributed to mesenchyme in E14.5 or E15.5 embryos, two-day-old mice, and adult mice (Fig. 4A, B). However, half of the BM mesenchyme was composed of cells other than P0/YFP$^+$ (Wnt1/YFP$^+$) and Mesp1/YFP$^+$ cells (Fig. 4A–C). Immunohistochemistry detected two-day-old P0/YFP$^+$ and Mesp1/YFP$^+$ BM mesenchymal cells in trabecular and cortical bone (Fig. 4B). Subsequently we reported that fetal thymic and dental mesenchymal cells have the potential to differentiate into melanocytes (a highly reliable marker of NC-derived cells) [31,32]. We confirmed the presence of NC-derived cells in BM, by testing whether these mesenchymal cells differentiate into melanocytes. Pigmented melanocytes were induced from YFP$^+$ cells in BM and YFP$^+$ cells from the skin of E17.5 *P0/YFP* embryos (Fig. 4D). The results suggested that NC-derived cells were present in the BM.

Next, we tested the expression of PDGFRs in BM mesenchymal cells. Unlike dental mesenchyme, PDGFRα- and/or PDGFRβ-expressing cells were present in the YFP$^+$ and YFP$^-$ fractions of BM mesenchymal cells from two-day-old *Mesp1/YFP* and *P0/YFP* mice (Fig. 4 C). The sections showed that two-day-old P0/YFP$^+$ BM mesenchymal cells around the blood vessels expressed α-SMA (Fig. 5A). Furthermore, Mesp1/YFP$^+$ BM mesenchymal cells of the same age expressed CD31 in blood vessels (Fig. 5B). Thus, NC-derived and mesoderm-derived cells in the BM may contribute to α-SMA$^+$ perivascular cells and CD31$^+$ endothelial cells, respectively.

In the thymus, most E13.5 thymic mesenchymal cells (except MHC class II$^+$ thymic epithelial cells) consisted of either Wnt1/YFP$^+$ or Mesp1/YFP$^+$ cells (Fig. 4E), while 86% of CD45$^-$Ter119$^-$ thymic mesenchymal cells from two-day-old mice were composed of either Wnt1/YFP$^+$ cells or Mesp1/YFP$^+$ cells (Fig. 4F). Similar to BM, PDGFRα- and/or PDGFRβ-expressing cells were observed in the YFP$^+$ and YFP$^-$ fractions of thymic mesenchymal cells from two-day-old *Mesp1/YFP* and *Wnt1/YFP* mice (Fig. 4F). The sections indicated that two-day-old Wnt1/YFP$^+$ thymic mesenchymal cells around the blood vessels expressed α-SMA, whereas Mesp1/YFP$^+$ thymic mesenchymal cells of the same age expressed CD31 in blood vessels (Fig. 5C, D). Thus, NC-derived and mesoderm-derived cells in the thymus may contribute to α-SMA$^+$ perivascular cells and CD31$^+$ endothelial cells, respectively.

Origins of BM and thymic CFU-Fs and roles of PDGFRs in these CFU-Fs

The observed discrepancy between PDGFR-expressing cells in the dental mesenchyme, the thymus, and the BM mesenchyme necessitated an assessment of CFU-F origins in the thymus and BM mesenchyme. We performed CFU-F assays using BM mesenchymal cells from two-day-old *Wnt1/YFP* (*P0/YFP*) and *Mesp1/YFP* mice. Unlike the dental mesenchymal cells, Mesp1/YFP$^+$ and Wnt1/YFP$^+$ (P0/YFP$^+$) BM mesenchymal cells exhibited colony-forming capacity (Fig. 6A). Unlike dental and thymic mesenchymal cells, it was unclear whether Mesp1/YFP$^-$ cells were Wnt1/YFP$^+$ (P0/YFP$^+$) NC-derived cells or whether Wnt1/YFP$^-$ (P0/YFP$^-$) cells were Mesp1/YFP$^+$ mesoderm-derived cells, because the mesenchymal cells comprised 1% Wnt1/YFP$^+$, 15% P0/YFP$^+$, and 27% Mesp1/YFP$^+$ cells, indicating that 57% of cells were not Wnt1/YFP$^+$ (P0/YFP$^+$) NC-derived cells or Mesp1/YFP$^+$ mesoderm-derived cells. Therefore, Wnt1/YFP$^-$ (P0/YFP$^-$) and Mesp1/YFP$^-$ mesoderm-derived cells may be present in BM (Figs. 4C, 6A), Nevertheless, Wnt1/YFP$^+$ and P0/YFP$^+$ cells comprised 44% and 85% of BM CFU-Fs, respectively (Fig. 6A, B). P0/YFP$^+$ BM mesenchymal cells from seven-month-old mice continued to exhibit a colony-forming capacity, and cells prepared from these colonies expressed PDGFRα and PDGFRβ (Fig. S4).

A secondary CFU-F assay was performed to investigate the self-renewal activity of BM CFU-Fs. Secondary CFU-Fs in the BM comprised 80% Wnt1/YFP$^+$ and 20% Wnt1/YFP$^-$ cells, or 100% Mesp1/YFP$^-$ cells (Fig. 6C, D). These results suggest that BM MSCs are derived mainly from NC and that they are maintained in older mice.

BM CFU-Fs were present in PDGFRα$^+$ and PDGFRβ$^+$ cells. Because the role of PDGFRs in BM CFU-Fs remained unclear; therefore, we examined the effects of anti-PDGFR antibodies on colony formation. Similar to dental CFU-Fs, the number of CFU-Fs induced from BM cells decreased with the addition of anti-PDGFRα and anti-PDGFRβ to the culture (Fig. 6A, B). The number of YFP$^+$ and YFP$^-$ colonies generated from BM mesenchymal cells of *P0/YFP*, *Wnt1/YFP* and *Mesp1/YFP* mice decreased (Fig. 6A, B). To assess the effects of these antibodies on the self-renewal capacity of CFU-Fs, we performed a primary CFU-F assay with anti-PDGFRβ and anti-PDGFRα antibodies, and a secondary CFU-F assay was performed without either antibody. In the BM mesenchymal cells from *Wnt1/YFP* mice, we found that the number of secondary colonies treated with both antibodies was 40% of that observed in the presence of the isotype control (Fig. 6C). The number of YFP$^+$ secondary colonies induced from the BM of *Wnt1/YFP* and *Mesp1/YFP* mice were reduced in the presence of both antibodies Fig. 6C, D). Irrespective of the origins of cells, it was clear that PDGFRβ signaling was important for maintaining self-renewal of BM CFU-Fs.

Next, we performed CFU-F assays using thymic mesenchymal cells from two-day-old *Wnt1/YFP* and *Mesp1/YFP* mice. Mesp1/YFP$^+$ and Wnt1/YFP$^-$ thymic mesenchymal cells exhibited colony-forming capacity (Fig. 6A). In particular, secondary CFU-Fs in the thymus were derived almost entirely from Mesp1/YFP$^+$ or Wnt1/YFP$^-$ cells (Fig. 6C, D). Similar to the BM CFU-Fs, the number of CFU-Fs induced from thymic cells decreased with the addition of anti-PDGFRα and anti-PDGFRβ to the culture (Fig. 6A, B). The number of YFP$^+$ and YFP$^-$ colonies generated using thymic mesenchymal cells from *Wnt1/YFP* and *Mesp1/YFP* mice decreased (Fig. 6A, B). Furthermore, thymic mesenchymal cells from *Wnt1/YFP* mice and *Mesp1/YFP* mice treated with anti-PDGFRα and anti-PDGFRβ antibody

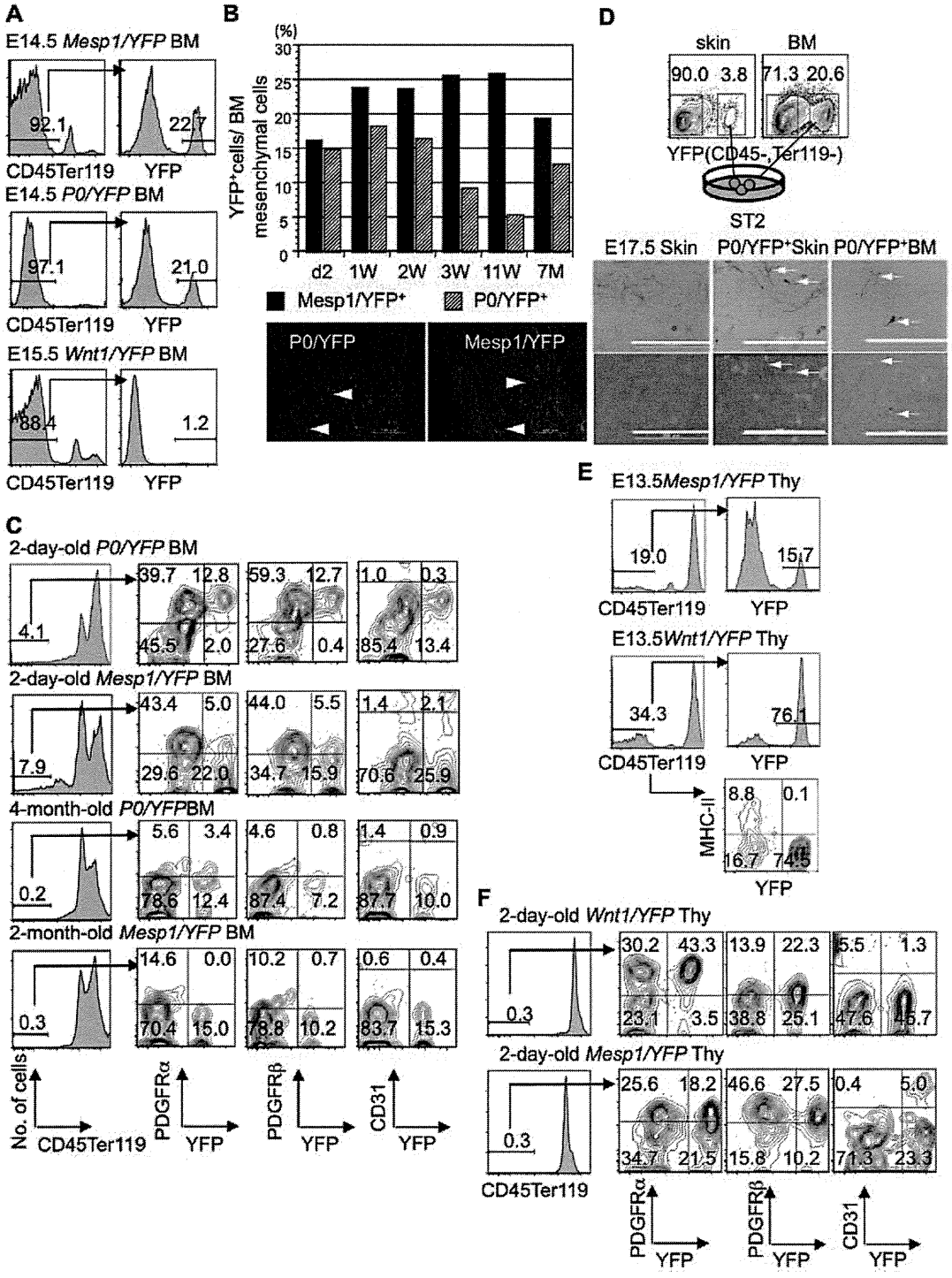

Figure 4. Origins and characteristics of mesenchymal cells in BM and thymus. (A) Contributions of YFP$^+$ mesenchymal cells from *Mesp1-Cre/YFP*, *P0-Cre/YFP*, and *Wnt1-Cre/YFP* embryos to BM. (B) YFP$^+$ cells from BM mesenchyme of *P0-Cre/YFP* and *Mesp1-Cre/YFP* mice from neonatal to adult stages. The mean of two independent experiments is shown. W, week; M, month. Immunohistochemistry for YFP in BM of 2-day-old *P0-Cre/YFP* and *Mesp1-Cre/YFP* mice (lower panel). White arrowheads indicate YFP$^+$ cells in the trabecular and cortical bone. (C) Expression of YFP, PDGFRα, PDGFRβ, and CD31 on BM mesenchymal cells prepared from *P0-Cre/YFP*, *Wnt1-Cre/YFP*, and *Mesp1-Cre/YFP* mice. (D) Induction of melanocytes from the sorted E17.5 P0/YFP$^+$ BM (6.5×10^3). The P0/YFP$^+$ cells from the skin of the same mice (P0/YFP$^+$ skin) and C57BL/6 mice were the controls. White arrows indicate pigmented and YFP$^+$ melanocytes. Scale bars, 200 μm. (E) Contributions of YFP$^+$ mesenchymal cells from *Mesp1-Cre/YFP* and *Wnt1-Cre/YFP* embryos to thymus. (F) Expression of YFP, PDGFRα, PDGFRβ, and CD31 on thymic mesenchymal cells prepared from *Wnt1-Cre/YFP*, and *Mesp1-Cre/YFP* mice. The experiments were repeated and one representative experiment is presented.
doi:10.1371/journal.pone.0046436.g004

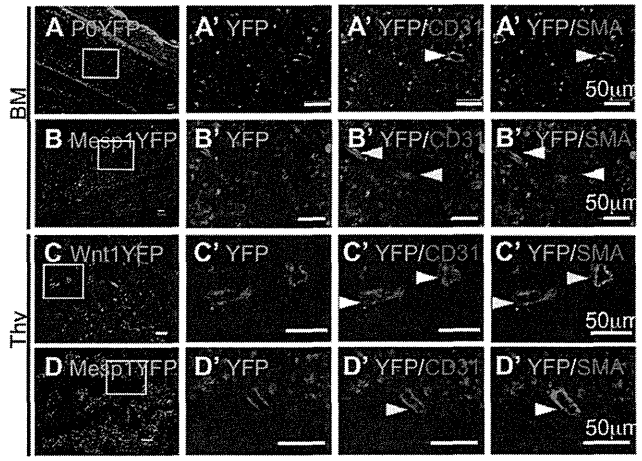

Figure 5. Immunohistochemistry of the BM or thymus of *P0-Cre/YFP*, *Mesp1-Cre/YFP*, and *Wnt1-Cre/YFP* mice. (A–D) Immunohistochemistry for YFP, CD31, and α-SMA in the BM (A, B) or thymus (C, D) of 2-day-old *P0-Cre/YFP* (A), *Mesp1-Cre/YFP* (B, D), and *Wnt1-Cre/YFP* (C) mice. High-magnification views (A'–D') of the boxed areas in (A–D), respectively. Yellow and white arrowheads indicate positive cells for each antibody to indicate the presence or absence of YFP^+ cells, respectively. Scale bars, 50 μm. The experiments were repeated and one representative experiment is presented.
doi:10.1371/journal.pone.0046436.g005

exhibited an unusual capacity for secondary colony formation (Fig. 6C, D). Similar to the BM, PDGFRβ signaling is important for maintaining thymic CFU-Fs containing self-renewal MSCs, irrespective of their origin.

BM and thymic mesenchymal cells can differentiate into osteoblasts, adipocytes, and chondrocytes

We cultured CFU-F progeny to assess the differentiation potential of BM and thymic mesenchymal cells and then found that CFU-F progeny from Wnt1/YFP^+($P0/YFP^+$) BM and thymic mesenchymal cells differentiated into osteoblasts, adipocytes, and chondrocytes (Fig. 6E). Unlike dental mesenchymal cells, Mesp1/YFP^+ BM and thymic mesenchymal cells had the potential to differentiate into osteoblasts and adipocytes (Fig. 6E). Thus, CFU-Fs with MSC properties develop mainly from NC and the mesoderm in the BM and thymic mesenchyme.

Dental mesenchymal cells support B lymphopoiesis and osteoclastogenesis

Dental and BM mesenchymal cells have many similarities. BM mesenchymal cells support the differentiation of B lymphocytes and osteoclasts [34,35]. However, it is unclear whether dental mesenchymal cells support the differentiation of these cells. Thus, we prepared dental and BM mesenchymal cells from three-day-old or nine-week-old *Wnt1/YFP* mice. First, we examined the expression of genes encoding the critical hematopoietic factors stem cell factor (SCF), interleukin-7 (IL-7), and CXC chemokine ligand 12 (CXCL12) [36]. Interestingly, dental mesenchyme expresses *Dentin sialophosphoprotein* (*Dspp*, which is an odontoblast-specific gene), *Mgf*, *Il7*, and *Cxcl12*, as does BM mesenchyme (Fig. 7A). To determine whether dental mesenchyme supported the differentiation of B lymphocytes, we prepared dental and BM mesenchymal cells from *Wnt1/YFP* mice. Two weeks later, 200 c-Kit^+ $Sca1^+$ $Lineage^-$ (KSL) cells were isolated from the BM of C57BL/6 mice were cultured in purified YFP^+ dental mesenchyme, which contained 94% YFP^+ cells, and unfractionated BM mesenchymal cells, which contained 18% YFP^+ cells with rmIL-7 (Fig. 7B). Two weeks later, we found that a large number of $CD19^+$ cells (B lineage cells) were induced on Wnt/YFP^+ dental mesenchymal cells (Y^+Tooth), BM mesenchymal cells (unfractionated BM), and ST2 cells, which support the differentiation of B lymphocytes and osteoclasts (Fig. 7B). Next, we studied the possible effects of Wnt/YFP^+ dental mesenchymal cells on osteoclast induction by culturing 100 KSL cells on these mesenchymal cells in the presence of $1\alpha,25(OH)_2D_3$ and Dex. After six days, we induced tartrate-resistant acid phosphatase $(TRAP)^+$ multinucleated osteoclasts on Wnt/YFP^+ dental mesenchymal, BM mesenchymal, and ST2 cells (Fig. 7C). We found that 94% of these dental mesenchymal cells were Wnt/YFP^+ NC-derived cells, which indicated that NC-derived dental mesenchymal cells had similar properties to BM mesenchymal cells in terms of their support of B lymphopoiesis and osteoclastogenesis.

Discussion

This study aimed to investigate the origin and characteristics of dental, thymic, and BM mesenchymal cells and MSCs. We used *Wnt1/YFP* and *P0/YFP* mice as markers of NC-derived cells and *Mesp1/YFP* mice as markers of mesoderm-derived cells. Most dental and thymic mesenchymal cells are composed of Wnt1/YFP^+ NC-derived cells or Mesp1/YFP^+ mesoderm-derived cells (Fig. 8). However, 57% BM mesenchyme comprises cells other than Wnt1/YFP^+ ($P0/YFP^+$) NC-derived cells or Mesp1/YFP^+ mesoderm-derived cells (Fig. 8). The lateral plate mesoderm (LPM) generates the limb skeleton [37]. Moreover, the *Mesp1* gene is expressed mainly in LPM-derived head mesenchyme and cardiac mesoderm. Therefore, expression of *Mesp1* gene may be insufficient to allow Cre-mediated recombination in LPM, or possibly other mesoderm-derived cells such as the paraxial mesoderm may contribute to LPM. The origin of BM mesenchymal cells may differ from that of dental and thymic mesenchymal cells.

Approximately similar numbers of $P0/YFP^+$ and Wnt1/YFP^+ cells were observed in the tooth and thymus, whereas larger numbers of $P0/YFP^+$ cells than Wnt1/YFP^+ cells were detected in BM. Although we cannot explain the difference between the numbers of YFP^+ cells, the fact that YFP^+ BM cells of *P0-Cre/Floxed-EGFP* and *Wnt1-Cre/Floxed-EGFP* mice differentiate into peripheral neurons and glia developing from NC [6], along with our observation that $P0/YFP^+$ and Wnt1/YFP^+ BM mesenchymal cells differentiate into melanocytes, suggests that *P0/YFP* and *Wnt1/YFP* mice mark NC-derived cells. Because *Wnt1-Cre* is expressed in early migratory NC [5,38], whereas *P0-Cre* is expressed in the early stage of NC cells and in the glial subset of NC cells [30,39], *P0/YFP* may also label other populations of NC-derived cells in addition to the common population of NC-derived cells labeled by both *P0/YFP* and *Wnt1/YFP* mice in BM. Alternatively, the discrepancy between *P0/YFP* and *Wnt1/YFP* mice may be attributed to a Cre-switching efficiency. However, YFP^+ BM mesenchymal cells in *Wnt1/YFP* demonstrated a marked capacity for colony formation, indicating that NC contributes to BM mesenchyme and its MSC. However, ectopic expression of the *P0-Cre* gene occurs in BM cells, because P0/YFP^+ cells were partially detected in hematopoietic cells and marked some non-NC–derived cells, including a minor population of endothelial cells in adult BM [40]. On the other hand, YFP^+ cells in *Sox1-Cre/YFP* mice, which help in tracing neuroepithelial cells, contribute to BM mesenchyme and BM MSCs [7]. The percentage of YFP^+ cells in BM mesenchyme of *Sox1-Cre/YFP*

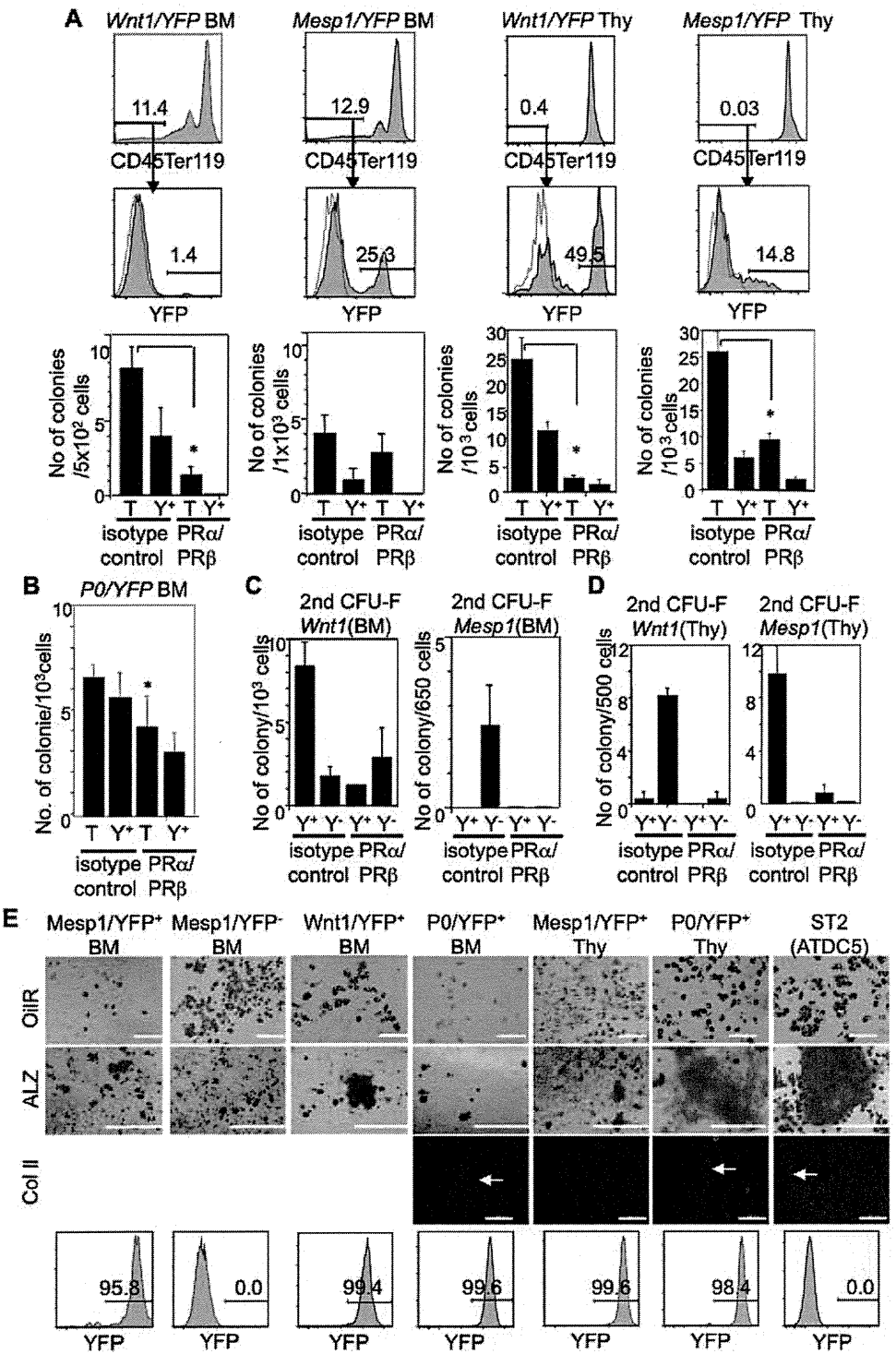

Figure 6. Origins and characteristics of BM and thymic CFU-Fs and roles of PDGFRs in these CFU-Fs. (A) Contributions of YFP$^+$ mesenchymal cells (CD45-Ter119-cells) from 2-day-old *Wnt1-Cre/YFP* and *Mesp1-Cre/YFP* mice to BM and thymus. BM and thymic CFU-F assays were performed in the presence of anti-PDGFRβ (APB5) and anti-PDGFRα (APA5) or isotype-matched control antibody. (B) Numbers of colonies induced from BM mesenchymal cells from 2-day-old *P0-Cre/YFP* mice in the presence of the anti-PDGFRβ and anti-PDGFRα. (C, D) The secondary CFU-F assay using cells from primary colonies induced from 1,000 BM (C) and thymic (D) mesenchymal cells of 2-day-old *Wnt1-Cre/YFP* and *Mesp1-Cre/YFP* mice in the presence of anti-PDGFRα and anti-PDGFRβ antibodies. The secondary CFU-F assay was performed in the absence of antibodies. T, total colonies; Y$^+$, YFP$^+$ colonies; Y$^-$, YFP$^-$ colonies. Values represent the mean (SD) of triplicate cultures. Asterisks indicate a significant difference in the number of colonies compared with that of the isotype-matched control antibody ($p<0.05$). (E) Differentiation potential of thymic and BM mesenchymal cells from *Wnt1-Cre/YFP*, *P0-Cre/YFP*, and *Mesp1-Cre/YFP* mice into adipocytes, osteoblasts, and chondrocytes. YFP expression in each cell preparation is shown in the lower panel. The cultured cells were stained with oil red O (OilR), alizarin red (ALZ), and anti-type II collagen (Col II) antibody to detect adipocytes, osteoblasts, and chondrocytes, respectively. ST2 and ATDC5 cells were the positive controls. The experiments were repeated twice and one representative experiment is presented. Scale bars, 200 μm in OilR and Col II in (E), and 1 mm in (ALZ in E). White arrows indicate positive cells against Col II antibody.

doi:10.1371/journal.pone.0046436.g006

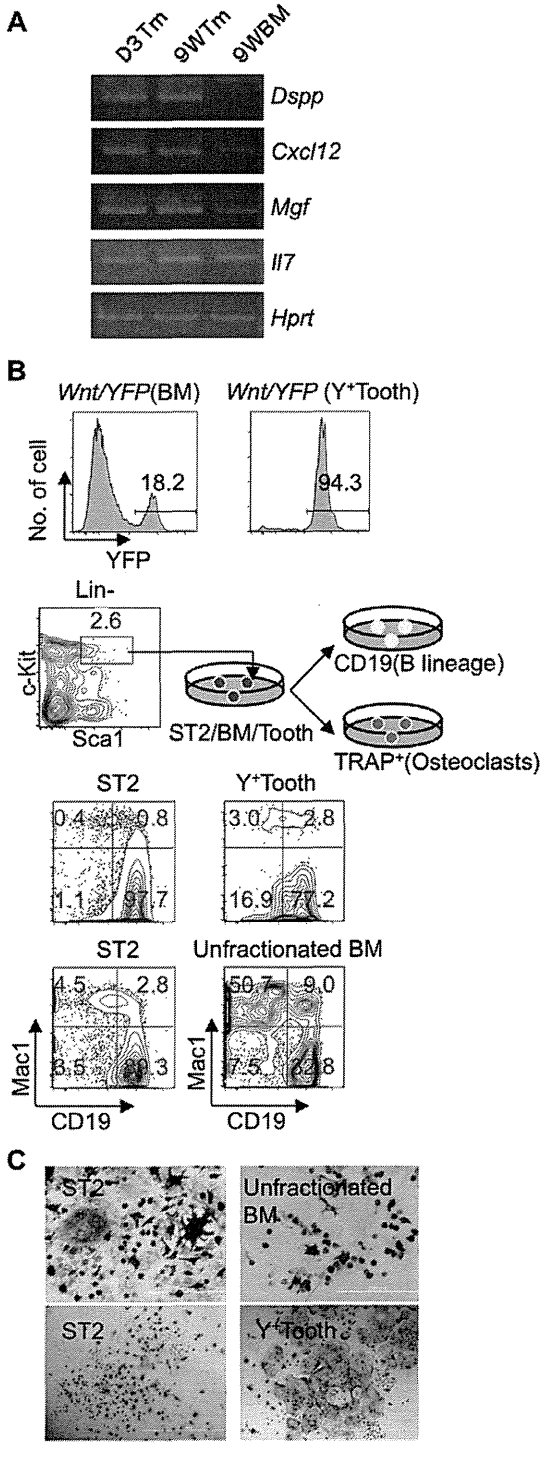

Figure 7. NC-derived dental mesenchymal cells support B lymphopoiesis and osteoclastogenesis. (A) Expression of genes encoding hematopoietic factors on CD45$^-$ and Ter119$^-$ BM mesenchymal cells and dental mesenchymal cells. RT-PCR was performed using RNA from these cells. Hypoxanthine guanidine phosphoribosyl transferase (*Hprt*) was the positive control. D3Tm, dental mesenchymal cells from 3-day-old mice; 9WTm, dental mesenchymal cells from 9-week-old mice; 9WBM, CD45$^-$ and Ter119$^-$ BM mesenchymal cells from 9-week-old mice. (B) Induction of B lineage cells. Unfractionated BM and purified YFP$^+$ dental mesenchymal cells (Y$^+$ Tooth) from 3-day-old *Wnt1-Cre/YFP* mice were cultured. Percentages of YFP$^+$ cells in the CD45$^-$ and Ter119$^-$ fractions after 2 weeks' culture (upper panels). BM-derived 200 KSL cells were then cultured on purified YFP$^+$ dental mesenchymal cells (Y$^+$ Tooth) or unfractionated BM mesenchymal cells in the presence of rmIL-7. Mac1 and CD19 were used as Myeloid cell lineage and B cell lineage markers. (C) Osteoclast induction. One hundred KSL cells were cultured on unfractionated BM and YFP$^+$ dental mesenchymal cells (Y$^+$ Tooth) prepared from the same mice in the presence of $1\alpha,25(OH)_2D_3$, and DEX. TRAP staining was performed to detect osteoclasts. ST2 stromal cells were used as the positive control to support the differentiation of B lymphocytes and osteoclasts. Each experiment with BM or dental mesenchyme is shown with ST2 as the control (B, C). Each experiment was repeated twice and one representative experiment is presented. Scale bars, 200 μm.
doi:10.1371/journal.pone.0046436.g007

mice was almost similar to that of YFP$^+$ cells from *Wnt1/YFP* mice.

The origins of dental pulp stem cells and stem cells from human exfoliated deciduous teeth (SHEDs) are unclear [16,19]. Because odontoblasts generally develop from NC, SHEDs that can differentiate into odontoblasts, osteoblasts, and neurons may develop from NC-derived cells. Contrary to our results, Iohara et al. reported that side population (SP) cells of adult porcine dental mesenchymal cells can differentiate into odontoblasts, chondrocytes, adipocytes, neurons, and endothelial cells [41]. These multipotent SP cells express CD31, CD34, FLK1, and CD105 (endothelial markers), but scarcely express α-SMA or NG2 (perivascular cell markers). Because endothelial cells are of mesodermal origin [42], these SP cells may be more immature than NC-derived cells or may comprise both NC-derived and mesoderm-derived cells.

Wnt1/YFP$^+$, unlike Mesp1/YFP$^+$ dental mesenchymal cells, exhibited marked potential for colony formation in the CFU-F assays. Because dental pulp includes small numbers of Mesp1/YFP$^+$ mesoderm-derived cells, we calculated the ratio of the number of YFP$^+$ colonies to the total number of YFP$^+$ mesenchymal cells in the CFU-F assays. The frequency of CFU-Fs within YFP$^+$ dental mesenchymal cells was lower than 1/2,040 (1/1,080) and 1/1,178 (1/728) in E13 (2-day-old) *Mesp1/YFP* and *Wnt1/YFP* mice, respectively. Mesp1/YFP$^+$ dental mesenchymal cells may rarely possess colony-forming capacity in the CFU-F assays. Although Mesp1/YFP$^+$ thymic and BM mesenchymal cells differentiate into adipocytes and osteoblasts, Mesp1/YFP$^+$ dental mesenchymal cells rarely differentiate into osteoblasts and chondrocytes *in vitro*, even when they successfully proliferate. Mesp1/YFP$^+$ mesoderm-derived cells in the dental mesenchyme may already have lost the potential to differentiate into osteoblasts and chondrocytes or be committed to endothelial cells.

Human dental pulp stem cells or SHEDs are similar to BM MSCs with regard to the expression of cell-surface antigens such as STRO1$^+$ and α-SMA$^+$ (perivascular cell markers) and CD146$^+$ (a perivascular cell and endothelial cell marker) [43]. In mouse dental pulp and BM cells, PDGFR-expressing cells have shown colony-forming capacity *in vitro*. However, unlike dental CFU-Fs, BM and thymic CFU-Fs comprise both Wnt1/YFP$^+$ (P0/YFP$^+$) NC-derived cells and Mesp1/YFP$^+$ mesoderm-derived cells. Furthermore, self-renewing CFU-Fs, including MSCs, consist entirely of Wnt1/YFP$^+$ (P0/YFP$^+$) NC-derived cells in the teeth, and mostly Wnt1/YFP$^+$ (P0/YFP$^+$) NC-derived cells in BM. We also showed that NC-derived dental mesenchymal cells expressed genes encoding critical hematopoietic factors such as IL-7, SCF, and CXCL12, and they supported the differentiation of B lymphocytes and osteoclasts [36,44]. Although it is unclear whether NC-derived and/or mesoderm-derived BM mesenchymal cells support B lymhopoiesis and osteoclasts, it is well known that cotransplantation of BM mesenchymal cells with hematopoietic cells promotes the reconstitution of hematopoiesis [45]. Because dental mesenchymal cells facilitate the easy preparation of MSCs compared

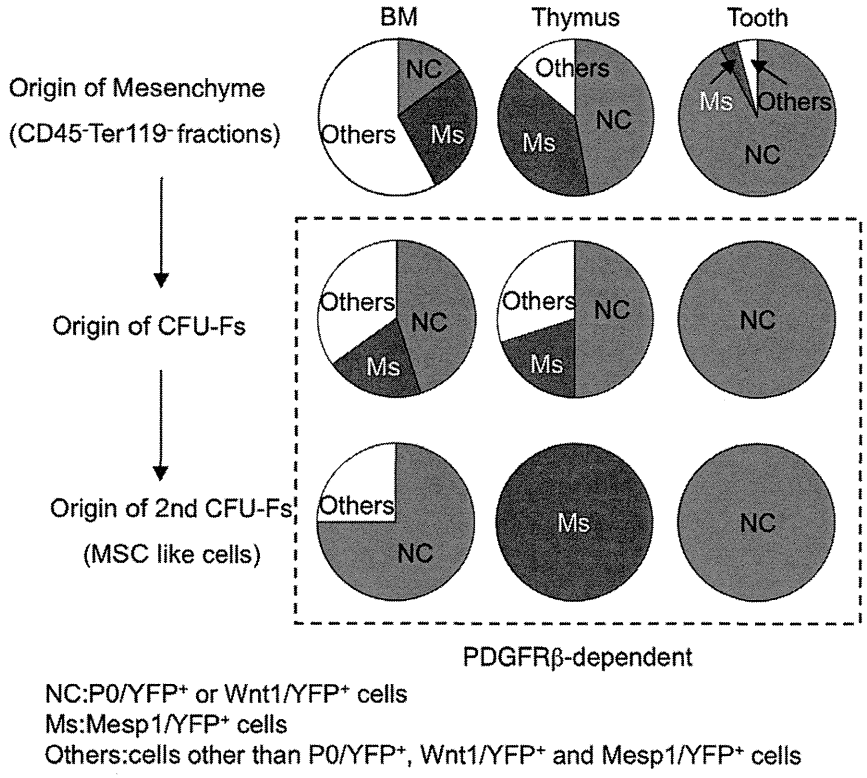

Figure 8. Origin and properties of dental, thymic, and BM mesenchymal cells and their CFU-Fs. Percentages of NC-derived and mesoderm-derived cells comprising BM, thymic, and dental mesenchyme (CD45$^-$ and Ter119$^-$ cells). YFP$^+$ cells in CD45$^-$ and Ter119$^-$ cells from *P0-Cre/YFP* and *Wnt1-Cre/YFP* mice represent NC-derived cells (NC). YFP$^+$ cells in CD45$^-$ and Ter119$^-$ cells from *Mesp1-Cre/YFP* mice represent mesoderm-derived cells (Ms). YFP$^-$ cells other than YFP$^+$ cells in the CD45$^-$ and Ter119$^-$ cells from *P0-Cre/YFP* (*Wnt1-Cre/YFP*) and *Mesp1-Cre/YFP* mice represent others. The expression of primary and secondary CFU-Fs *in vitro* was dramatically affected by PDGFRβ inhibition, irrespective of tissue and origin.
doi:10.1371/journal.pone.0046436.g008

with BM stromal cells, dental mesenchyme may represent a useful resource in improving hematopoiesis in patients with hematopoietic disorders. However, it is still not clear the role of NC-derived cells or mesoderm-derived cells in the BM and thymic lympho-hematopoiesis. Further examination is desire to elucidate these roles.

We first indicated that an inhibitory antibody against PDGFRβ decreased the CFU-F count. Retention of 15% CFU-Fs generated in the control culture in the presence of anti-PDGFRβ implies that both PDGFRβ-dependent and PDGFRβ-independent CFU-Fs are present in the dental pulp, BM, and thymus. Simultaneous addition of anti-PDGFRα and anti-PDGFRβ more effectively blocked secondary colony formation in dental and thymic CFU-F progeny. Because PDGFRα is upregulated in response to *Pdgfrb* mutation [46], anti-PDGFRβ–treated cells may increase PDGFRα expression and become sensitive to anti-PDGFRα.

Conclusion

This is the first report to demonstrate that both NC-derived and mesoderm-derived cells with CFU-F capacity contribute to the dental pulp, thymus, and BM from the fetal stage to the adult stage. Although the origin of self-renewing CFU-Fs differs by tissue, these CFU-Fs are dependent on PDGFRβ irrespective of their origin.

Materials and Methods

Animals and Ethics Statement

P0-Cre, *Wnt1-Cre*, and *Rosa26EYFP* mice were provided by Drs. K. Yamamura (Kumamoto University), H. Sucov (Southern California University), and H. Enomoto (RIKEN Kobe), respectively [47]. *Mesp1-Cre* and C57BL/6 mice were obtained from the Riken Bioresource Center and Clea Japan, Inc., respectively. All mice were maintained at the Institute of Laboratory Animals, Mie University; all experimental procedures were approved by the Institutional Animal Care and Use Committee of Mie University (approval number 20–22), and were performed according to the Mie University guidelines for laboratory animals.

Preparation of single-cell suspensions

The mandibular molar tooth buds and dental pulp of the lower incisors were incubated with 2.4 U dispase II (Roche) in 10% FBS/HBSS for 30 min at 4°C and 1 mg/mL collagenase D (Roche) in 10% FBS/HBSS for 2 h at 37°C. Thymi were incubated with 1 mg/mL collagenase D in 10% FBS/HBSS for 1 h at 37°C. Femora and tibia were minced and were incubated with 2.0 U dispase II and 0.1 mg/mL collagenase D in 10% FBS/HBSS for 1 h at 37°C, and then in 2% FBS/HBSS for 1 h at 37°C. The dorsal regions of E9.5 embryos were dissected and incubated with 2.4 U dispase II in 10% FBS/HBSS at 4°C for 1 h, minced, and then incubated with 1 mg/mL collagenase D in

10% FBS/HBSS for 1 h at 37°C. Pipetted single-cell suspensions were used for further procedures.

RNA isolation and RT-PCR

Total RNA was prepared using Trizol (Invitrogen). cDNA synthesis was carried out using reverse transcriptase (RevertraAce; Toyobo) and oligo (dT) primers (Toyobo). PCR using cDNA was performed with r*Taq* polymerase (Toyobo) and the forward primers and reverse primers were as follows: *AP2*: 5′-AGGGACTTTGGGTACGTGTG-3′, 5′-AGGGCCTGGGTGAGATAGTT-3′; *p75(NGFR)*: 5′-TGCTGCTGCTGCTGCTGCTGCTTCT-3′, 5′-CGGGTCCACGTGGTTGGCTTCATCT-3′; *Sox10*: 5′-CACTACACCGACCAGCCGTCCACTT-3′, 5′-GATAGAGTCGTATATACTGGCTGCT-3′; *Krox20*: 5′-ACCCCTGGATCTCCCGTATCCGAGT-3′, 5′-GGACAGGGAAACGGCTTTCGATCTG-3′; *Brachyury(T)*: 5′-CTCCAACCTATGCGGACAAT-3′, 5′-CCCCTTCATACATCGGAGAA-3′; *Dentin sialophosphoprotein(Dspp)*: 5′-ACATTGTTGAAAACTCTGTGGCTGTGCCTC-3′, 5′-CATTTGCTGTGCTGTTCTCTCCTCTCGCAT-3′; *Il7*: 5′-ACATCATCTGAGTGCCACA-3′, 5′-CTCTCAGTAGTCTCTTTAG-3′; *Mgf*: 5′-GTGGCAAATCTTCCAAATGA-3′, 5′-CTCGGGACCTAATGTTGAAG-3′; *Cxcl12*: 5′-GCTCTGCATCAGTGACGGTAAAC-3′, 5′-GCAATATCGTACCATATGCTATGGC-3′; *Hprt*: 5′-AGTTCTTTGCTGACCTGCTG-3′, 5′-GCTTTGTATTGGGCTTTTCC-3′. PCR was performed as follows: 94°C for 4 min; 35 cycles at 93°C for 1 min, 55°C (*Mgf, Cxcl12*), 56°C (*Il7*), 58°C (*Sox10, Dspp, Hprt*), 60°C (*AP2, Krox20, Brachyury*), 63°C (*p75*) for 1 min, and 72°C for 1 min; and extension at 72°C for 7 min.

Antibodies

The following antibodies were used: biotin-conjugated PDGFRβ (APB5; eBioscience); Pacific Blue-conjugated streptavidin (eBioscience); APC-conjugated PDGFRα (APA5; eBioscience), PDGFRβ (APB5), CD31 (PECAM1) (MEC13.3; eBioscience), Mac1 (M1/70; Biolegend), and c-Kit (2B8; eBioscience); Cy7PE-conjugated CD45 (30-F11; eBioscience), Ter119 (eBioscience), and CD19 (6D5; Biolegend); Pacific Blue-conjugated Sca1 (Ly-6 A/E) (E13-161.7; Biolegend); PE-conjugated MHC Class II (I-Ab) (25-9-17; BD Pharmingen), FLK1 (Avasα1; eBioscience), and CD34 (RAM34; BD Pharmingen); rabbit anti-mouse p75NGFR polyclonal antibody (Chemicon); Alexafluor 405-conjugated goat anti-rabbit IgG (Invitrogen); biotin-conjugated CD4 (GK1.5; eBioscience), CD8α (53-6.7; eBioscience), Mac1 (M1/70), Gr1 (RB6-8C5; eBioscience), B220 (6B2; eBioscience), and Ter119; and PE-conjugated streptavidin.

Cell sorting and analysis

Cells were analyzed on FACS Aria or FACS Canto II (BD), followed by analyses with FlowJo software (Tree Star).

Immunohistochemistry

Molar tooth germs, lower incisors, thymi, and femora were fixed in 4% paraformaldehyde and embedded in cryomold for sectioning (10 μm). The following antibodies were used: Alexafluor 488-conjugated rabbit anti-GFP IgG (Invitrogen), rat anti-mouse CD31 (PECAM-1) (MEC13.3), DyLight™ 649-conjugated AffiniPure donkey anti-rat IgG (H+L) (Jackson ImmunoResearch Laboratory), Cy3-conjugated mouse anti–α-smooth muscle actin (α-SMA) (1A4) (Sigma), mouse anti–neuron-specific β-tubulin III (TUJ1; Babco), and Cy3-conjugated AffiniPure donkey anti-mouse polyclonal IgG (HL) (Jackson ImmunoResearch Laboratory). Images were captured using confocal microscopy (Olympus FV1000D).

CFU-F assays

Mesenchymal cells from tooth buds, dental pulp, BM, and thymi of *P0-Cre/YFP*, *Wnt1-Cre/YFP*, and *Mesp1-Cre/YFP* mice were cultured in α-MEM with 20% FBS in 6-well plates in the presence/absence of inhibitory antibodies against PDGFRα (anti-PDGFRα, APA5) [48] and/or PDGFRβ (anti-PDGFRβ, APB5) [49]; antibodies against c-Kit (ACK4) and IL-7Rα (A7R) were used as isotype-matched controls in BM and thymic cultures, respectively. Inhibitory antibodies against c-Fms (AFS98) were used to inhibit macrophage proliferation. Two weeks later, large (>50 cells) and small colonies (clusters <50 cells) and YFP^+ and YFP^- colonies were scored as primary CFU-Fs [17]. For secondary CFU-F assays to detect self-renewing CFU-Fs, cells from primary colonies were cultured in the presence/absence of antibodies. Selected YFP^+/YFP^- primary colonies were cultured to establish YFP^+ clones.

Induction of adipocytes, osteoblasts, and chondrocytes

For osteoblast induction, 100,000 cells were cultured in DMEM medium (Gibco) supplemented with 10% FBS, 10^{-7} M Dexamethasone (DEX; Sigma), 40 nM human ascorbic acid 2 phosphatase (Sigma), 1 nM BMP4 (Neomarker), and 10 mM β-glycerophosphate (Sigma) [32,50]. For adipocyte induction, 100,000 cells were cultured in α-MEM supplemented with 10% FBS, 0.25 μM DEX, 0.5 mM 3-isobutyl-1-methylxanthine (Sigma), 1 μM Triiodo (Sigma), and 0.2 μ M insulin (Sigma) [51]. For chondrocyte induction, 200,000 cells (1×10^7/mL) were cultured in α-MEM supplemented with 10% FBS, 10^{-7} M DEX, 40 nM ascorbic acid-2-phosphatase, and 1 nM TGFβ3 or BMP2 (Neomarker) [49]. After 2–3 weeks, cells were stained with oil red-O (OilR), alizarin red (ALZ), and mouse anti-type II collagen antibody (6B3, Neomarker) and Cy3-conjugated goat anti-mouse IgG (Jackson ImmunoResearch Laboratory) to detect adipocytes, osteoblasts, and chondrocytes, respectively. ST2 and ATDC5 cells were the positive controls for osteogenesis and adipogenesis, and chondrogenesis, respectively [52].

Induction of B lymphocytes and osteoclasts

Dental and BM mesenchymal cells were prepared from 3-day-old *Wnt1-Cre/YFP* mice. Femoral c-Kit^+ $Sca1^+$ $Lineage^-$ (KSL) cells were isolated from 8-week-old C57BL/6 mice. For B lymphocyte induction, 200 KSL cells were cultured on purified YFP^+ dental mesenchymal cells or unfractionated BM mesenchymal cells in RPMI-1640 (Gibco) supplemented with 10% FBS, 5×10^{-5} M 2ME, and 10 ng/mL rmIL-7 (Invitrogen). After 2 weeks, cells collected were analyzed by FACS. For osteoclast induction, 100 KSL cells were cultured on these mesenchymal cells in α-MEM supplemented 10% FBS, 10^{-7} M DEX, and 10^{-7} M 1α, 25-dihydroxyvitamin D ($1\alpha,25(OH)_2D_3$) (Biomol Research Laboratory). After 6 days, TRAP activity of cells was studied to detect osteoclasts [34]. ST2 cells were the positive control used for the differentiation of B lymphocytes and osteoclasts [34,35].

Induction of melanocytes from BM mesenchymal cells

Single-cell suspensions from BM of *P0-Cre/YFP* embryos were prepared. Sorted YFP^+ BM mesenchymal cells from *P0-Cre/YFP* embryos (20,000) were cultured on ST2 cells in α-MEM containing 10% FBS with 10^{-7} M DEX, 20 pM rhbFGF (R&D Systems), 10 pM cholera toxin (Sigma), and 40 nM rhET3

(Peptide Institute) [31]. Skin YFP$^+$ cells of the same mice were used as a positive control. The pigmented melanocytes were microscopically examined after 3 weeks.

Statistical analysis

Data are expressed as means (SD). Statistical significance was assessed using Student's *t*-test.

Supporting Information

Figure S1 Expression of NC- and mesoderm-associated genes on cells from *P0-Cre/YFP*, *Wnt1-Cre/YFP*, and *Mesp1-Cre/YFP* mice. (A) Expression of p75NGFR on cells in the CD45$^-$ and Ter119$^-$ fractions from E9.5 *P0-Cre/YFP* and *Wnt1-Cre/YFP* embryos. Empty means secondary antibody only (Alexafluor 405-conjugated goat anti-rabbit IgG) without primary antibody. (B) Expression of NC-associated genes on cells from E9.5 *P0-Cre/YFP*, *Wnt1-Cre/YFP*, and *Mesp1-Cre/YFP* embryos ($n=4$/group). (C) Expression of NC- and mesoderm-associated genes in dental mesenchymal cells from *Wnt1-Cre/YFP* mice ($n=4$/group). YFP$^+$ and YFP$^-$ cells were isolated using a cell sorter. RT-PCR was performed using RNA from these cells. Hypoxanthine guanidine phosphoribosyl transferase (*Hprt*) was the positive control; no expression was detected without a template (data not shown).
(TIF)

Figure S2 Expression of cell-surface antigens related to endothelial cells on dental mesenchymal cells from 4-week-old *Wnt1-Cre/YFP* and *Mesp1-Cre/YFP* mice. Expression of cell-surface antigens related to endothelial cells on YFP$^+$ or YFP$^-$ dental mesenchymal cells in CD45$^-$ and Ter119$^-$ fractions from 4-week-old *Wnt1-Cre/YFP* and *Mesp1-Cre/YFP* mice. The experiments were repeated twice and one representative experiment is presented.
(TIF)

Figure S3 Expression of PDGFR and CD31 on dental mesenchymal cells from CFU-F progenies of 4-week-old *Mesp1-Cre/YFP* or *Wnt1-Cre/YFP* mice. (A) Number of colonies in the tertiary CFU-F assay using YFP$^-$ and YFP$^+$ dental mesenchymal cells isolated from secondary CFU-F progenies from *Mesp1-Cre/YFP* mice. Values represent the mean (SD) of triplicate cultures. (B) Expression of PDGFRa and PDGFRβ on YFP$^-$ and YFP$^+$ dental mesenchymal cells from secondary CFU-F progenies from *Mesp1-Cre/YFP* mice. (C) Expression of CD31 and PDGFRβ on YFP$^+$ and YFP$^-$ cells recovered from primary CFU-F progenies from *Mesp1-Cre/YFP* and *Wnt1-Cre/YFP* mice. The experiments were repeated twice and one representative experiment is presented.
(TIF)

Figure S4 CFU-Fs of BM mesenchymal cells from 7-month-old *P0-Cre/YFP* mice. (A) Numbers of colonies induced from BM mesenchymal cells from 7-month-old *P0-Cre/YFP* mice. (B) Expression of YFP, PDGFRα, and PDGFRβ on cells from these colonies. Values represent the mean (SD) of triplicate cultures. The experiments were repeated twice and one representative experiment is presented.
(TIF)

Table S1 The number of primary and secondary colonies and the origin of colony-forming cells in dental mesenchymal cells. Numbers of primary colonies (1st CFU-F, >50 cells) induced from 4×10^3 dental mesenchymal cells from 4-week-old *Wnt1-Cre/YFP* and *Mesp1-Cre/YFP* mice. Numbers of secondary colonies (2nd CFU-F, >50 cells) induced from 1×10^3 primary colonies of 4-week-old mice. Values represent the means (SD) of triplicate cultures. Asterisks indicate total number of colonies obtained from triplicate cultures of two independent experiments.
(DOC)

Table S2 Effects of inhibitory antibodies against PDGFRs in CFU-F assays using dental mesenchymal cells. Numbers of colonies were induced from 8×10^3 dental mesenchymal cells prepared from 4-week-old *Wnt1-Cre/YFP* mice in the presence of inhibitory antibody against PDGFRα (APA5) and/or inhibitory antibody against PDGFRβ (APB5). No add means no antibody, and control means isotype-matched control antibody (ACK4). All antibodies were used in 10 mg/ml. Numbers of large (L, >50 cells), small (clusters) (S, <50 cells), and total colonies (T, L+S colonies) are shown. Values represent the means (SD) of triplicate cultures. Asterisks indicate a significant difference from the number of colonies in the presence of the isotype-matched control antibody ($p<0.05$). The experiments were repeated twice and one representative experiment is presented.
(DOC)

Acknowledgments

We thank Drs. S. Iseki and T. Shigeoka for their helpful discussion; Drs. K. Yamamura, H. Sucov, and H. Enomoto for providing the *P0-Cre*, *Wnt1-Cre*, and *Rosa26EYFP* mice; Dr. S. Nishikawa for providing the monoclonal antibodies (ACK4, A7R, and AFS98); and Ms. Yamada for technical assistance. The authors would like to thank Enago (www.enago.jp) for the English language review.

Author Contributions

Conceived and designed the experiments: HY TY. Performed the experiments: YK DK KI HY. Analyzed the data: HY TY. Contributed reagents/materials/analysis tools: NT. Wrote the paper: HY TY SH.

References

1. Anderson DJ (1997) Cellular and molecular biology of neural crest cell lineage determination. Trends Genet 13: 276–280.
2. Le Douarin NM, Kalcheim C (1999) Cell lineage segregation during neural crest ontogeny. The Neural Crest. In: Le Douarin NM, Kalcheim, C eds. Cambridge: Cambridge University Press. pp. 304–335.
3. Bockman DE, Kirby ML (1984) Dependence of thymus development on derivatives of the neural crest. Science 223: 498–500.
4. Le Douarin NM, Jotereau FV (1975) Tracing of cells of the avian thymus through embryonic life in interspecific chimeras. J Exp Med 142:17–40.
5. Jiang X, Rowitch DH, Soriano P, McMahon AP, Sucov HM (2000) Fate of the mammalian cardiac neural crest. Development 127: 1607–1616.
6. Nagoshi N, Shibata S, Kubota Y, Nakamura M, Nagai Y, et al. (2008) Ontogeny and multipotency of neural crest-derived stem cells in mouse bone marrow, dorsal root ganglia, and whisker pad. Cell Stem Cell 2: 392–403.
7. Takashima Y, Era T, Nakao K, Kondo S, Kasuga M, et al. (2007) Neuroepithelial cells supply an initial transient wave of MSC differentiation. Cell 129: 1377–1388.
8. Etchevers HC, Vincent C, Le Douarin NM, Couly GF (2001) The cephalic neural crest provides pericytes and smooth muscle cells to all blood vessels of the face and forebrain. Development 128: 1059–1068.
9. Yoshida T, Vivatbutsiri P, Morriss-Kay G, Saga Y, Iseki S (2008) Cell lineage in mammalian craniofacial mesenchyme. Mech Dev 125: 797–808.
10. Foster K, Sheridan J, Veiga-Fernandes H, Roderick K, Pachnis V, et al. (2008) Contribution of neural crest-derived cells in the embryonic and adult thymus. J Immunol 180: 3183–3189.
11. Chung UI, Kawaguchi H, Takato T, Nakamura K (2004) Distinct osteogenic mechanisms of bones of distinct origins. J Orthop Sci 9: 410–414.
12. Couly GF, Coltey PM, Le Douarin NM (1993) The triple origin of skull in higher vertebrates: a study in quail-chick chimeras. Development: 117: 409–429.

13. Harel I, Nathan E, Tirosh-Finkel L (2009) Distinct origins and genetic programs of head muscle satellite cells. Dev Cell 16: 822–832.
14. McBratney-Owen B, Iseki S, Bamforth SD, Olsen BR, Morriss-Kay GM (2008) Development and tissue origins of the mammalian cranial base. Dev Biol: 322: 121–132.
15. Matsuoka T, Ahlberg PE, Kessaris N, Iannarelli P, Dennehy U, et al. (2005) Neural crest origins of the neck and shoulder. Nature 436: 347–355.
16. Gronthos S, Mankani M, Brahim J, Robey PG, Shi S (2000) Postnatal human dental pulp stem cells (DPSCs) in vitro and in vivo. Proc Natl Acad Sci U S A 97: 13625–13630.
17. Friedenstein AJ, Chailakhjan RK, Lalykina KS (1970) The development of fibroblast colonies in monolayer cultures of guinea-pig bone marrow and spleen cells. Cell Tissue Kinet 13: 393–403.
18. Jiang Y, Jahagirdar BN, Reinhardt RL, Schwartz RE, Keene CD, et al. (2002) Pluripotency of mesenchymal stem cells derived from adult marrow. Nature 418: 41–49.
19. Miura M, Gronthos S, Zhao M, Lu B, Fisher LW, et al. (2003) SHED: stem cells from human exfoliated deciduous teeth. Proc Natl Acad Sci U S A 100: 5807–5812.
20. Pittenger MF, Mackay AM, Beck SC, Jaiswal RK, Douglas R, et al. (1999) Multilineage potential of adult human mesenchymal stem cells. Science 284: 143–147.
21. Kruger GM, Mosher JT, Bixby S, Joseph N, Iwashita T, et al. (2002) Neural crest stem cells persist in the adult gut but undergo changes in self-renewal, neuronal subtype potential, and factor responsiveness. Neuron 35: 657–669.
22. Morikawa S, Mabuchi Y, Kubota Y, Nagai Y, Niibe K, et al. (2009) Prospective identification, isolation, and systemic transplantation of multipotent mesenchymal stem cells in murine bone marrow. J Exp Med 206: 2483–2496.
23. Morrison SJ, White PM, Zock C, Anderson DJ (1999) Prospective identification, isolation by flow cytometry, and in vivo self-renewal of multipotent mammalian neural crest stem cells. Cell 96: 737–749.
24. Morikawa S, Mabuchi Y, Niibe K, Suzuki S, Nagoshi N, et al. (2009) Development of mesenchymal stem cells partially originate from the neural crest. Biochem Biophys Res Commun 379: 1114–1119.
25. Sieber-Blum M, Grim M, Hu YF, Szeder V (2004) Pluripotent neural crest stem cells in the adult hair follicle. Dev Dyn 231: 258–269.
26. Wong CE, Paratore C, Dours-Zimmermann MT, Rochat A, Pietri T, et al. (2006) Neural crest-derived cells with stem cell features can be traced back to multiple lineages in the adult skin. J Cell Biol 175:1005–1015.
27. Chai Y, Jiang X, Ito Y, Bringas P Jr, Han J, et al. (2000) Fate of mammalian cranial neural crest during tooth and mandibular morphogenesis. Development 127: 1671–1679.
28. Saga Y, Miyagawa-Tomita S, Takagi A, Kitajima S, Miyazaki J, et al. (1999) MesP1 is expressed in the heart precursor cells and required for the formation of a single heart tube. Development 126: 3437–3447.
29. Soriano P (1999) Generalized lacZ expression with the ROSA26 Cre reporter strain. Nat Genet 21: 70–71.
30. Yamauchi Y, Abe K, Mantani A, Hitoshi Y, Suzuki M, et al. (1999) A novel transgenic technique that allows specific marking of the neural crest cell lineage in mice. Dev Biol 212: 191–203.
31. Yamazaki H, Sakata E, Yamane T, Yanagisawa A, Abe K, et al. (2005) Presence and distribution of neural crest-derived cells in the murine developing thymus and their potential for differentiation. Int Immunol 17: 549–558.
32. Yamazaki H, Tsuneto M, Yoshino M, Yamamura K, Hayashi S (2007) Potential of dental mesenchymal cells in developing teeth. Stem Cells 25: 78–87.
33. Gronthos S, Simmons PJ (1995) The growth factor requirements of STRO-1-positive human bone marrow stromal precursors under serum-deprived conditions in vitro. Blood 85(4): 929–940.
34. Yamazaki H, Kunisada T, Yamane T, Hayashi S (2001) Presence of osteoclast precursors in colonies cloned in the presence of hematopoietic colony-stimulating factors. Exp Hematol 29: 68–76.
35. Nishikawa S, Ogawa M, Nishikawa S, Kunisada T, Kodama H (1988) B lymphopoiesis on stromal cell clone: stromal cell clones acting on different stages of B cell differentiation. Eur J Immunol 18: 1767–1771.
36. Tagaya H, Kunisada T, Yamazaki H, Yamane T, Tokuhisa T, et al. (2000) Intramedullary and extramedullary B lymphopoiesis in osteopetrotic mice. Blood 95(11): 3363–3370.
37. Gilbert SF (2010) Chapter 11, Paraxial mesoderm and intermediate mesoderm. Developmental Biology, 9th Edition. In: Carol Wigg ed. Sinauer Associates Inc. pp. 413–444.
38. Echelard Y, Vassileva G, McMahon AP (1994) Cis-acting regulatory sequences governing Wnt-1 expression in the developing mouse CNS. Development 120(8): 2213–2224.
39. Messing A, Behringer RR, Hammang JP, Palmiter RD, Brinster RL, et al. (1992) P0 promoter directs expression of reporter and toxin genes to Schwann cells of transgenic mice. Neuron 8(3): 507–520.
40. Kubota Y, Takubo K, Hirashima M, Nagoshi N, Kishi K, et al. (2011) Isolation and function of mouse tissue resident vascular precursors marked by myelin protein zero. J Exp Med 208(5): 949–960.
41. Iohara K, Zheng L, Ito M, Tomokiyo A, Matsushita K, et al. (2006) Side population cells isolated from porcine dental pulp tissue with self-renewal and multipotency for dentinogenesis, chondrogenesis, adipogenesis, and neurogenesis. Stem Cells 24: 2493–2503.
42. Hirashima M, Kataoka H, Nishikawa S, Matsuyoshi N, Nishikawa S (1999) Maturation of embryonic stem cells into endothelial cells in an in vitro model of vasculogenesis. Blood 93: 1253–1263.
43. Shi S, Gronthos S (2003) Perivascular niche of postnatal mesenchymal stem cells in human bone marrow and dental pulp. J Bone Miner Res 18: 696–704.
44. Sugiyama T, Kohara H, Noda M, Nagasawa T (2006) Maintenance of the hematopoietic stem cell pool by CXCL12-CXCR4 chemokine signaling in bone marrow stromal cell niches. Immunity 25(6): 977–988.
45. Bensidhoum M, Chapel A, Francois S, Demarquay C, Mazurier C, et al. (2004) Homing of in vitro expanded Stro-1− or Stro-1+ human mesenchymal stem cells into the NOD/SCID mouse and their role in supporting human CD34 cell engraftment. Blood 103(9): 3313–3319.
46. Soriano P (1994) Abnormal kidney development and hematological disorders in PDGF beta-receptor mutant mice. Genes Dev 8:1888–1896.
47. Srinivas S, Watanabe T, Lin CS, William CM, Tanabe Y, et al. (2001) Cre reporter strains produced by targeted insertion of EYFP and ECFP into the ROSA26 locus. BMC Dev Biol 1, 4
48. Takakura N, Yoshida H, Ogura Y, Kataoka N, Nishikawa S, et al. (1997) PDGFR alpha expression during mouse embryogenesis: immunolocalization analyzed by whole-mount immunohistostaining using the monoclonal anti-mouse PDGFR alpha antibody APA5. J Histochem Cytochem 45: 883–893.
49. Sano H, Sudo T, Yokode M, Murayama T, Kataoka N, et al. (2001) Functional blockade of platelet-derived growth factor receptor-beta but not of receptor-alpha prevents vascular smooth muscle cell accumulation in fibrous cap lesions in apolipoprotein E-deficient mice. Circulation 103: 2955–2960.
50. Kramer J, Hegert C, Rohwedel J (2003) In vitro differentiation of mouse ES cells: bone and cartilage. Methods Enzymol 365: 251–268.
51. Dani C, Smith AG, Dessolin S, Leroy P, Staccini L, et al. (1997) Differentiation of embryonic stem cells into adipocytes in vitro. J Cell Sci 110: 1279–1285.
52. Atsumi T, Miwa Y, Kimata K, Ikawa Y (1990) A chondrogenic cell line derived from a differentiating culture of AT805 teratocarcinoma cells. Cell Differ Dev 30: 109–116.

Cell PRESS

Immunity
Article

The Transcription Factor Jdp2 Controls Bone Homeostasis and Antibacterial Immunity by Regulating Osteoclast and Neutrophil Differentiation

Kenta Maruyama,[1] Masahiro Fukasaka,[1] Alexis Vandenbon,[2] Tatsuya Saitoh,[1] Takumi Kawasaki,[1] Takeshi Kondo,[1] Kazunari K. Yokoyama,[4] Hiroyasu Kidoya,[3] Nobuyuki Takakura,[3] Daron Standley,[2] Osamu Takeuchi,[1,5] and Shizuo Akira[1,3,*]

[1]Laboratory of Host Defense
[2]Laboratoy of Systems Immunology, WPI Immunology Frontier Research Center (IFReC)
[3]Research Institute for Microbial Diseases
Osaka University, Osaka 565-0871, Japan
[4]Cancer Center, Kaohsiung Medical University Hospital, 807 Kaohsiung, Taiwan
[5]Laboratory of Infection and Prevention, Institute for Virus Research, Kyoto University, Kyoto 606-8507, Japan
*Correspondence: sakira@biken.osaka-u.ac.jp
http://dx.doi.org/10.1016/j.immuni.2012.08.022

SUMMARY

Jdp2 is an AP-1 family transcription factor that regulates the epigenetic status of histones. Previous in vitro studies revealed that Jdp2 is involved in osteoclastogenesis. However, the roles of Jdp2 in vivo and its pleiotropic functions are largely unknown. Here we generated *Jdp2*$^{-/-}$ mice and discovered its crucial roles not only in bone metabolism but also in differentiation of neutrophils. *Jdp2*$^{-/-}$ mice exhibited osteopetrosis resulting from impaired osteoclastogenesis. *Jdp2*$^{-/-}$ neutrophils were morphologically normal but had impaired surface expression of Ly6G, bactericidal function, and apoptosis. We also found that ATF3 was an inhibitor of neutrophil differentiation and that Jdp2 directly suppresses its expression via inhibition of histone acetylation. Strikingly, *Jdp2*$^{-/-}$ mice were highly susceptible to *Staphylococcus aureus* and *Candida albicans* infection. Thus, Jdp2 plays pivotal roles in in vivo bone homeostasis and host defense by regulating osteoclast and neutrophil differentiation.

INTRODUCTION

Jun dimerization protein 2 (Jdp2) is a member of the AP-1 family and interacts with other AP-1 components, such as c-Jun, JunB, JunD, and ATF2 (Aronheim et al., 1997). Jdp2 can inhibit the activation of its binding partners, suggesting that it is a transcriptional repressor (Jin et al., 2001). Furthermore, Jdp2 suppresses histone acetyltransferase activity and acetylation of reconstituted nucleosomes, thereby regulating the epigenetic status of histones (Jin et al., 2006). Extensive studies have revealed that Jdp2 plays roles in various cellular responses, such as UV-induced apoptosis and osteoclastogenesis (Huang et al., 2010).

Osteoclasts are multinucleated cells that degrade bone (Karsenty and Wagner, 2002). Bone-forming osteoblasts express macrophage colony-stimulating factor (M-CSF) and RANK ligand (RANKL). When these cytokines stimulate their receptors, c-fms and RANK, respectively, transcription factors such as c-Fos, NF-κB, and NFATc1 (Takayanagi, 2007) are activated in osteoclast precursors and osteoclastogenesis is induced by stimulation of osteoclastogenic genes, such as tartrate-resistant acid phosphatase (TRAP) and cathepsin K (CTSK). Jdp2 was previously implicated in positive regulation of osteoclastogenesis via activation of the TRAP and CTSK promoters (Kawaida et al., 2003). Recent findings indicate that the Jdp2 locus is hypomethylated and that its transcript is upregulated in common myeloid precursors and granulocyte-macrophage progenitors relative to lymphoid lineages (Ji et al., 2010), suggesting that Jdp2 may also contribute to the differentiation of myeloid cells, such as neutrophils.

Neutrophils are critical for bacterial clearance. One of the most impressive morphological features of mature neutrophils is cytosolic granules, and the mRNA expressions of granule content genes are significantly higher in immature neutrophils than in mature neutrophils (Borregaard and Cowland, 1997; Borregaard et al., 2007). There are three different granule subtypes, i.e., primary, secondary, and tertiary, and the granule proteins play pivotal roles in bacterial killing. The other bactericidal agents derived from neutrophils are reactive oxygen species (ROS), such as superoxide (Forman and Thomas, 1986). Recently, a novel mechanism of bacterial and fungal killing mediated by chromatin structures was elucidated, termed the neutrophil extracellular trap (NET) (Brinkmann et al., 2004). This extracellular structure is released through a cell death requiring ROS production (Nishinaka et al., 2011) and chromatin decondensation (Li et al., 2010). Collectively, these findings demonstrate that neutrophils exert bactericidal activity through several complex machineries.

Generally, neutrophil subtypes can be distinguished by their surface markers CD11b and Ly6G. CD11b^{+}Ly6G^{lo} cells are immature neutrophils with a round nucleus, such as myelocytes, whereas CD11b^{+}Ly6G^{hi} cells are band-segmented mature neutrophils (Hestdal et al., 1991). By using such morphological and molecular cues, several studies have shown that various cytokines and transcription factors are critical for proper